Available online at www.sciencedirect.com
ScienceDirect
Lithos 91 (2006) 352–372
LITHOS
www.elsevier.com/locate/lithos

Subsolidus deuteric/hydrothermal alteration of eudialyte in lujavrite from the Pilansberg alkaline complex, South Africa

Roger H. Mitchell *, Ruslan P. Liferovich

Department of Geology, Lakehead University, 955 Oliver Road, Thunder Bay, Ontario, Canada P7B 5E1

Received 29 March 2005; accepted 13 March 2006
Available online 16 June 2006

Abstract

The most evolved rocks of the Pilansberg alkaline complex are aegirine lujavrites in which three varieties of eudialyte are recognized on the basis of textural relationships and composition. Manganoan eudialyte-I is a relict orthomagmatic phase occurring as poikilitic plates or as relict grains in pseudomorphed euhedral phenocrysts. Late eudialyte-II ranges in composition from manganoan eudialyte through kentbrooksite to taseqite-like varieties and is considered to be formed by cation exchange with eudialyte-I and alkaline fluids. Eudialyte-III is a hydrothermal phase replacing eudialyte-II, and has either taseqite-like (5–7.3 wt.% SrO, <2.0 wt.% REE_2O_3) or kentbrooksite (<1.5 wt.% SrO, ~8.5 wt.% REE_2O_3) compositions. Three styles of replacement of eudialyte-I and -II are recognizable. Type 1 involves replacement by complex aggregates of zircon, fergusonite-(Ce), allanite-(Ce), britholite-(Ce), titanite, pyrochlore, albite and potassium feldspar, i.e. a "miaskitic" paragenesis. Type 2 alteration consists of complex aggregates dominated by deuteric Na–Zr-silicates (?catapleiite), stronalsite, strontium-apatite and lamprophyllite replacing eudialyte-I and -II and relicts of the "miaskitic paragenesis", i.e. a highly sodic "agpaitic-to-hyperagpaitic" paragenesis. Type 3 replacement involves mantling of any residual eudialyte-II and zircon, and replacement of deuteric Na–Zr-silicates by eudialyte-III together with barytolamprophyllite as late hydrothermal phases. Further alteration and replacement resulted in the superposition of natrolite, britholite, pyrochlore, allanite and diverse Ba- and Mn-based minerals onto the types 2 and 3 assemblages, and ultimately to the deposition of allanite-(La), La-dominant REE carbonates and rarely a silica phase. All of the alteration styles are considered to have occurred in situ under subsolidus conditions (<450 °C) by interaction of pre-existing eudialyte and other minerals with deuteric, sodium- and chlorine-bearing aqueous fluids. The evolution of the replacement products is from a miaskitic through an agpaitic to a hyperagpaitic paragenesis and ultimately back to a low agpaitic-to-miaskitic assemblage, reflecting changes in the $a(Na^+)/a(Cl^-)$ ratio and alkalinity of the deuteric/hydrothermal fluids.

Keywords: Pilansberg; Eudialyte; Lujavrite; Autometasomatic; Alteration

1. Introduction

The Mesoproterozoic Pilansberg agpaitic alkaline complex is a large (~25×24 km) partially unroofed ring intrusion that was emplaced at an intraplate extensional structure along a contact between granitic and noritic units of the Bushveld massif, South Africa. The geology of the Pilansberg complex is as yet inadequately characterized, the only significant studies being those of: Shand (1928), Retief (1962, 1963), Ferguson (1973) and Lurie (1973, 1986). The only modern mineralogical investigations are those of Olivo and Williams-Jones

* Corresponding author. Tel.: +1 807 343 8287; fax: +1 807 346 7853.
E-mail address: rmitchel@lakeheadu.ca (R.H. Mitchell).

0024-4937/$ - see front matter © 2006 Elsevier B.V. All rights reserved.
doi:10.1016/j.lithos.2006.03.025

(1999) on hydrothermal REE–Mn–Nb-rich eudialyte and Mitchell and Liferovich (2004) on ecandrewsite–pyrophanite solid solutions.

The complex consists of phonolitic-to-trachytic pyroclastic units and lavas, intruded by diverse nepheline syenites, i.e. the red, white and green foyaites of Shand (1928), together with tinguaite dikes and large cone sheets. Many of the Pilansberg syenites have petrographic and mineralogical affinities to lujavrite, khibinite and foyaite occurring in the Khibina and Lovozero peralkaline complexes.

We have studied a suite of lujavrites collected from the central and southern parts of the complex with the objective of characterizing the subsolidus alteration of eudialyte and other primary minerals, and correlating the mineralogical changes observed with the model developed by Markl and Baumgartner (2002) for the evolution of the alkalinity of deuteric fluids interacting with their parental sodic agpaitic syenites.

2. Lujavrite

The "green foyaite" of Shand (1928) is the youngest of the Pilansberg syenites (Lurie, 1986). These rocks occur primarily as arcuate ring dike-like units in the north and south of the complex and as a small intrusion in the core of the complex. The rocks exhibit a very wide range of textures and modes as a result of flow differentiation, crystal sorting and accumulation.

Four textural varieties of eudialyte-bearing agpaitic nepheline syenite were examined in this study. Many of these exhibit trachytic textures resulting from flow-alignment of alkali feldspar and aegirine phenocrysts (Fig. 1a), and are similar to lujavrite from the type locality at Lovozero, Russia (Ramsay, 1894). The areal distribution and inter-relationships between the various textural types is not known, as there have not been any modern detailed field investigations of the complex. In this work, all of the "green foyaites" which are characterized by the presence of alkali feldspar, albite, nepheline, sodalite, eudialyte, aegirine, sodic amphibole and astrophyllite–kupletskite as primary minerals, are termed, lujavrite (sensu lato), regardless of their texture (Mitchell, 1996). Although the abundance of major and accessory minerals varies considerably between textural types, we consider that all are derived from similar magmas and are thus consanguineous because of: (i) the compositional similarity of the major and accessory minerals present; (ii) the similar compositional trends observed for major, minor and accessory phases; and (iii) identical modes of subsolidus evolution.

Aegirine lujavrite (sensu lato) consists of prismatic aegirine and potassium feldspar plates which are flow-aligned. The minerals have an irregular modal distribution, which results in the formation of meso-to-melanocratic bands, 0.3–0.5 m in thickness, with gradational contacts. Rosettes and subparallel needle-like aggregates of green aegirine form the matrix of the rock and impregnate centimetre-sized plates of alkali feldspar (25–30 vol.%), stubby nepheline or sodalite (15–20 vol.%) and eudialyte (10–15 vol.%). Astrophyllite and lamprophyllite (5–10 vol.%.) occur as 0.5–2 cm poikilitic laths. Black prismatic aegirine and amphibole are rare. Eudialyte appears as altered anhedral grains or as small euhedral crystals, which for the most part are pseudomorphed by complex mixtures of secondary deuteric minerals. The latter includes strongly pleochroic purple-to-violet eudialyte of the latest generation (see below). Primary albite is not present in the lujavrite. Opaque minerals occur as grains of 0.01–0.5 mm in size or fine-grained aggregates in conjunction with altered eudialyte and sorosilicates.

The lujavrite has been subjected to successive recrystallization and replacement of nepheline and/or alkali feldspar, initially by sodalite, then by banalsite–stronalsite solid solution and analcime, and ultimately by natrolite (Fig. 1b). The intensity of these processes varies from site-to-site, and nepheline and sodalite are completely altered in some samples.

A variety of lujavrite apparently lacking alkali feldspar but rich in sodalite and eudialyte (each up to 20–25 vol.%) is termed here "melanolujavrite". In places, melanolujavrite contains albite laths that are co-aligned with acicular aegirine or poikilitically enclosed by crystals of eudialyte and nepheline. This albite-bearing melanolujavrite is similar to the eudialyte-bearing "green nepheline syenite" described by Olivo and Williams-Jones (1999). Euhedral plates of K-feldspar in this rock are scarce and contain abundant acicular crystals of aegirine. Eudialyte, which is characteristically altered, occurs as single, formerly euhedral, microphenocrysts (0.05–2 mm) or fine-grained aggregates of secondary phases in which relicts of pale rose-coloured eudialyte are evident in thin section. Eudialyte is replaced by complex mixtures of zeolites, alkali feldspar, opaque phases, titanite, zircon, unidentified deuteric Na–Zr-silicates (termed here NZS phases) and strongly pleochroic deep-purple to violet hydrothermal eudialyte similar to that described by Olivo and Williams-Jones (1999). In addition to the euhedral pseudomorphs, the rock also contains anhedral "domains", up to 0.8 cm in size, consisting of the same secondary mineral assemblage, thus suggesting the

former presence of larger anhedral grains of eudialyte which have been completely replaced. In places, the rock contains coarse-grained leucocratic lenses or bands (2–3 cm in thickness) consisting mainly of nepheline coexisting with up to 20–30 vol.% eudialyte and 10–15 vol.% aegirine. These bands have gradational transitions to the host melanolujavrite.

Rocks which have textural variations ranging from inequigranular-to-porphyritic on a decimetre scale are collectively termed here heterogeneous lujavrite. Commonly, the inequigranular varieties are similar to aegirine lujavrite (sensu lato) in mode and have incipiently trachytic and foliated textures. Some samples of inequigranular lujavrite do not contain eudialyte, whereas others contain rosenbuschite and keldyshite-like minerals together with eudialyte. In places, albite becomes abundant together with black prismatic arfvedsonite, and felted or rosette-like aggregates of aegirine. We consider these rocks to be transitional to "Ledig foyaite" (Lurie, 1986). Some coarse-grained varieties of the heterogeneous lujavrite contain star-like aggregates of black aegirine and large crystals of microcline, with relatively abundant albite and fluorite. These varieties of inequigranular lujavrite and those transitional to "Ledig foyaite" are not considered further here.

In the least-altered inequigranular lujavrite, two varieties of eudialyte are observed. One occurs as anhedral poikilitic grains measuring 0.1–2.5 cm in size which enclose nepheline (partially or entirely replaced by sodalite) and early-forming clinopyroxene-I (see below) (Fig. 1c). A second is represented by small (0.02–0.2 mm) euhedral crystals (Fig. 1d). The large poikilitic grains are in the most instances totally altered and replaced by a fine-grained mixture of zircon, britholite, pyrochlore, fergusonite, analcime and NZS phase(s). The euhedral crystals are observed to entrap these aggregates formed by means of alteration of poikilitic eudialyte (Fig. 1d) and, in turn, were subject to deuteric break-down and pseudomorphing.

Porphyritic lujavrite is the most variable variety in modal composition and consists principally of alkali feldspar phenocrysts set in a medium- to coarse-grained matrix of nepheline, potassium feldspar, aegirine, sodalite and analcime. The alkali feldspar in these rocks is similar to all other alkali feldspars in composition and consists of ordered microcline (see below). In some porphyritic varieties, alkali feldspar accounts for less than 5 vol.% and the porphyritic texture results from the presence of large subhedral nepheline crystals. Sodalite commonly entirely replaces nepheline and comprises up to 15–20 vol.%. Varieties transitional to inequigranular lujavrite are common.

Postmagmatic processes have resulted in the corrosion and replacement of primary minerals in all of the lujavrites investigated. Leaching voids and cavities were not observed, implying that the alteration was "volume-conserving" and thus similar to the autometasomatic alteration processes described by Markl and Baumgartner (2002) in lujavrite from the Ilímaussaq complex.

Our limited field observations did not indicate the separate development or presence of other alkaline fluids, e.g. development of late-stage hydrothermal veins, mineralized shear zones, compositionally contrasting small intrusions or dykes. These observations imply a consanguineous origin for the deuteric fluids and the autometasomatic character of the postmagmatic processes in the lujvarites.

3. Analytical methods

All mineral compositions were determined at Lakehead University by quantitative energy dispersive X-ray spectrometry (EDXA) using a JEOL JSM-5900LV scanning electron microscope (SEM) equipped with a Link ISIS 300 analytical system incorporating a Super ATW Light Element Detector (133 eV FwHm Mn*K*). Raw X-ray spectra were acquired for 130 s (live time) with an accelerating voltage of 20 kV and beam current of 0.475 nA on a Ni standard. Spectra were processed with the Link ISIS SEMQUANT quantitative analysis software package with full ZAF corrections applied. The following well-characterized mineral and synthetic standards were employed: benitoite (Ba), fluoroapatite

Fig. 1. Some characteristic textures and mineral relationships observed in Pilansberg lujavrite. Photomicrographs in plane-polarized light (a–d) and back-scattered electron images (e–h). (a) Common trachytoid texture of lujavrite; (b) stepwise alteration of an euhedral nepheline crystal with consecutive replacement by banalsite–stronalsite solid solution series, analcime and finally by natrolite; (c) large anhedral grain of poikilitic eudialyte-I in heterogeneous lujavrite; (d) an euhedral crystal of eudialyte-II which entraps fine-grained products of alteration of precursor eudialyte-I in the core; (e) eudialyte-I oikocryst enclosing euhedral nepheline chadacrysts (partially converted to sodalite), alkali feldspar and clinopyroxene; (f) clinopyroxene crystal mantling and replacing (?) amphibole; (g) clinopyroxene oikocryst enclosing euhedral nepheline chadacrysts which are partially converted to sodalite; (h) texture similar to (e) with eudialyte being converted to an unidentified deuteric Na–Zr–Si phase(s) (NZS). Mineral generations are given in Roman numerals: An = analcime, BS = banalsite–stronalsite solid solution series, Cpx = clinopyroxene, Eud = eudialyte, KFsp = potassic feldspar, Lm = lamprophyllite, MArf = mafnesioarfvedsonite, Ne = nepheline, NZS = an unidentified catapleiite-like deuteric Na–Zr-silicate phase(s), Sod = sodalite.

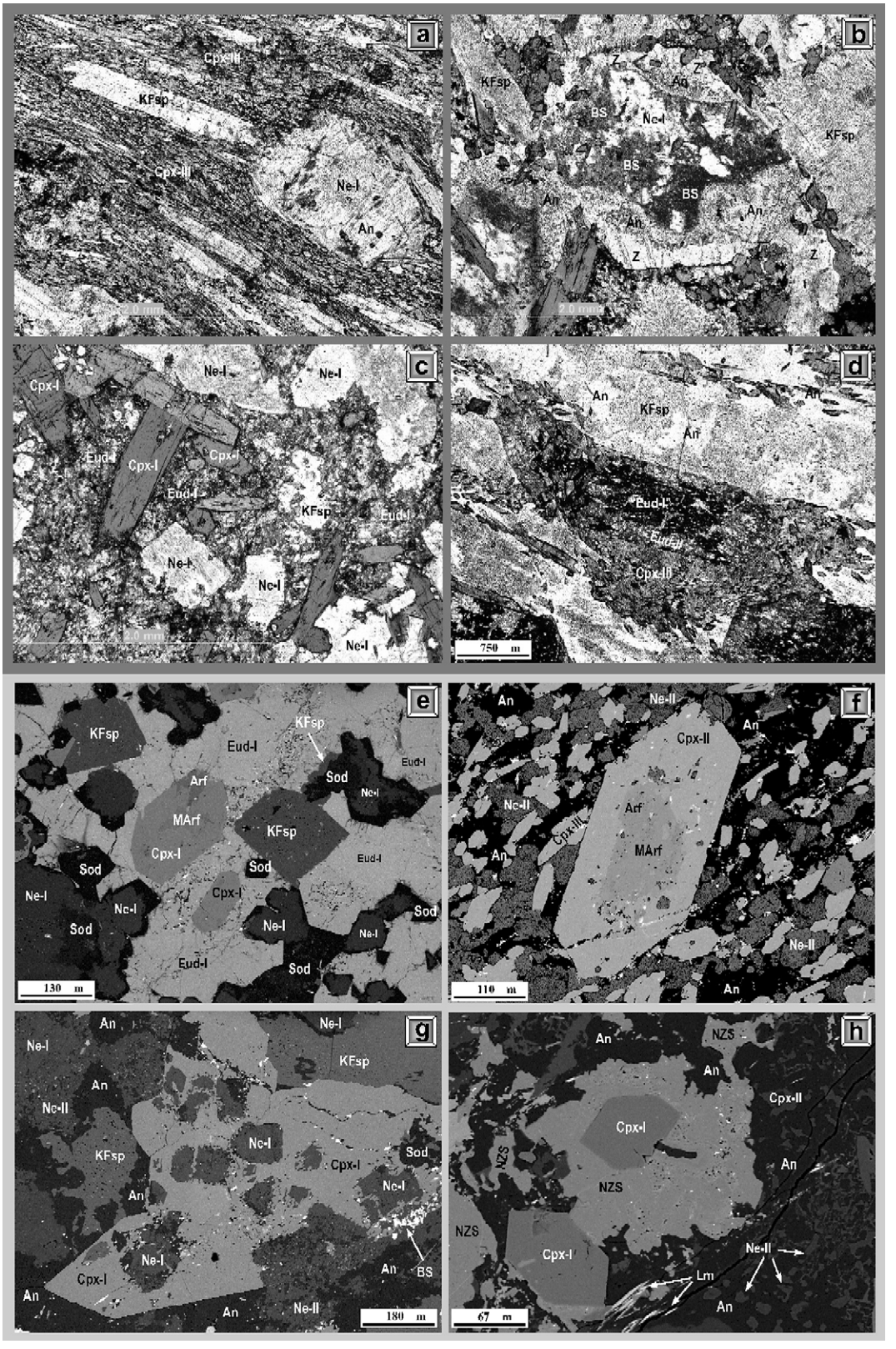
a
Cpx-III
KFsp
Cpx-II
Ne-I
An
b
KFsp
Z
Aeg
BS
Ne-I
KFsp
BS
An
BS
An
An
Z
Z
c
Ne-I
Ne-I
Cpx-I
Eud-I
Cpx-I
Cpx-I
Eud-I
KFsp
Eud-I
Ne-I
Ne-I
Ne-I
d
An
KFsp
An
An
Eud-I
Eud-II
Cpx-III
750 m
e
KFsp
KFsp
Eud-I
Eud-I
Sod
Arf
Ne-I
MArf
KFsp
Cpx-I
Sod
Sod
Eud-I
Ne-I
Cpx-I
Ne-I
Sod
Sod
Ne-I
Ne-I
Eud-I
Sod
130 m
f
An
Ne-II
Cpx-II
An
Ne-II
Arf
Cpx-II
An
MArf
Ne-II
An
110 m
g
An
Ne-I
Ne-I
KFsp
An
Ne-II
Ne-I
KFsp
Cpx-I
Sod
Ne-I
An
Ne-I
Cpx-I
An
BS
An
An
Ne-II
180 m
h
An
NZS
An
Cpx-II
Cpx-I
NZS
An
NZS
NZS
Cpx-I
Ne-II
Lm
An
67 m

(F, P, Ca in apatite), corundum (Al), jadeite (Na), silicate glass DJ-35 (Na, Mg, Si, Ca in pyroxene), ilmenite (Ti, Fe), Mn-fayalite (Mn), loparite (La, Ce, Pr, Nd), lueshite (Nb), orthoclase (K), periclase (Mg), NaCl (Cl), $SrTiO_3$ (Sr), zircon (Zr). A multi-element standard was used for the rare earth elements (REE) as with EDXA spectrum-stripping techniques it provides more accurate data than single REE standards. However, peak profiles used for analytical lines were obtained using fluoride standards for individual REE. The accuracy of the EDXA methods employed here has been cross-checked and confirmed by means of wave-length dispersion electron probe microanalysis (WDS EPMA) using automated CAMECA SX-50 microprobes located at Purdue University (West Lafayette, Indiana) and the University of Manitoba (Winnipeg) following methods described by Mitchell and Vladykin (1996) and Chakhmouradian and Mitchell (2002).

Particular care was taken during the analysis to avoid volatilization of Na by using raster scanning over a 5×5 to 10×10 μm area and reducing the counting time to 60 s. The reliability of the Na analyses was cross-checked by analysing natrolite every 1.5 h. Fluorine was observed to be present in eudialyte, mica and other minerals, but was not analysed quantitatively because of the overlap of F$K\alpha$ peaks with the $L\alpha$ peaks of transition metals in energy dispersive spectra.

The method of Droop (1987) was used to recalculate microprobe-obtained total Fe to ferric and ferrous iron. The apparent absence of Fe^{3+} in some minerals, in particular amphibole, is considered to be a consequence of incomplete analysis due to the presence of light elements such as Li or Be.

A powder X-ray diffraction study of hand-separated, HCl-washed (Wilkinson, 1965) alkali feldspar was undertaken using a Philips 3710 diffractometer operated in step-scan mode (Cu$K\alpha$ radiation; 2θ range 10–145°, 0.02° $\Delta 2\theta$; 4 s step). The degree of ordering of the alkali feldspar was determined from the separation of the 131 and $1\bar{3}1$ diffraction peaks.

4. Major primary silicates and accessory minerals—paragenesis and compositions

4.1. Amphibole

Amphibole occurs primarily as a relict phase, which is corroded and replaced by aegirine (clinopyroxene-III and -IV, see below) and as an apparently primary phase overgrowing aegirine augite (clinopyroxene-I). The earliest amphibole is eckermannite (mg#=0.66), which grades through magnesio-arfvedsonite (mg#=0.48) to arfvedsonite (mg#=0.42) (Table 1, comp. 1–3; Fig. 1e, f). The latter amphiboles occur intergrown with tainiolite in one sample of heterogeneous lujavrite and might contain some undetermined lithium.

4.2. Clinopyroxene

Clinopyroxenes are the principal primary mafic constituents (30–50 vol.%) of the lujavrites and occur in four texturally distinct generations ranging in composition from early euhedral aegirine–augite to acicular flow-aligned aegirine. Relict amphiboles mantled by aegirine occur in some samples (Fig. 1f). Clinopyroxene-I occurs as black euhedral prisms and aggregates that poikilitically enclose nepheline (Fig. 1g). Clinopyroxene-I is commonly fragmented, resorbed and replaced by later generations of pyroxene and rarely by biotite. Clinopyroxene-II forms slender prisms up to 0.5 mm in length or mantles corroded crystals of amphibole and clinopyroxene-I and commonly encloses corroded titanite. The most abundant pyroxene is acicular clinopyroxene-III, which occurs as flow-aligned aggregates (Fig. 1a,d) and growing into crystals of associated minerals. The last generation to crystallize is thin acicular clinopyroxene-IV, which occurs in altered alkali feldspar and natrolite or forms mantles upon earlier-crystallized pyroxenes. On the basis of their textural relationships, clinopyroxene-I and -II are considered as primary magmatic minerals, whereas clinopyroxene-III and -IV are of postmagmatic origin. Retief (1962) considers that clinopyroxene-IV in feldspar results from the alteration of Fe- and Na-bearing alkali feldspar under subsolidus conditions. A similar paragenetic sequence of clinopyroxene crystallization has been described from agpaitic nepheline syenite occurring at Gordon Butte, Montana, by Chakhmouradian and Mitchell (2002).

Clinopyroxene-I, the least evolved variety in terms of Na, Mg and Fe content, is an alumina-poor aegirine augite (Table 1, comp. 4 and 5; Fig. 2a). Clinopyroxene-II is alumina-poor titanian aegirine augite (Table 1, comp. 6; Fig. 2a). Clinopyroxene-III is aegirine with low CaO and TiO_2 contents (Table 1, comp. 7; Fig. 2a). Clinopyroxene-IV is near-stoichiometric aegirine (Table 1, comp. 8; Fig. 2a). The Zr content of the clinopyroxenes is typically below the detection limit of the EDXA analysis method but can reach ~1 wt.% ZrO_2 in aegirine mantling late zirconosilicates.

Fig. 2a shows that all clinopyroxenes in the Pilansberg lujavrite are highly evolved in terms of Na, Fe, Ca and Mg contents, and grade from primary magmatic aegirine–augite ($Ae_{57}Di_{19}Hd_{24}$) to hydrothermal aegirine (Ae_{100}).

Table 1
Representative compositions of some major minerals and minor phases

	1	2	3	4	5	6	7	8	9	10	11	12	13	14	15
Na_2O	8.05	7.13	7.46	7.29	8.68	10.52	11.05	12.38	1.57	1.74	10.32	9.99	1.08	0.80	0.16
K_2O	1.64	1.98	–2.50	–	–	–	–	–	6.86	6.55	0.77	1.50	0.35	8.21	11.70
CaO	3.95	2.46	2.32	10.27	7.50	4.69	2.73	0.36	1.86	2.14	–	0.20	0.20	1.12	–
SrO	–	0.62	–	–	–	–	–	–	–	0.45	17.66	3.78	–	–	–
BaO	–	–	–	–	–	–	–	–	–	–	1.80	21.10	26.20	–	–
MgO	14.08	9.27	8.81	3.17	2.58	1.27	1.14	–	0.64	0.51	–	–	0.26	2.12	19.46
MnO	1.86	2.04	1.93	1.14	0.99	0.65	1.58	–	14.41	19.13	5.08	3.91	15.63	5.61	0.20
FeO[a]	12.94	14.67	17.29	7.17	5.08	1.72	0.05	0.29	21.74	16.14	–	–	–	29.49	0.41
Al_2O_3	0.77	1.45	1.56	0.52	0.68	0.74	0.66	1.73	1.33	1.37	0.41	0.27	–	9.95	0.47
TiO_2	0.52	1.51	1.68	0.92	1.02	1.92	2.99	0.34	11.92	11.96	26.70	28.34	14.79	3.64	0.67
Nb_2O_5	–	–	–	–	–	–	–	–	0.16	0.35	0.47	–	1.51	–	–
SiO_2	55.29	50.10	51.48	51.28	51.61	52.08	52.14	52.20	35.44	35.70	30.72	28.97	24.26	35.79	58.73
Fe_2O_3[b]	0.03	3.86	2.50	18.78	22.36	27.10	28.47	31.90	–	–	1.83	1.61	11.14	–	–
Li_2O[b]	–	–	–	–	–	–	–	–	–	–	–	–	–	–	3.99
Total	99.13	94.47	97.53	100.54	100.50	100.69	100.81	99.20	96.15	96.04	97.86[c]	100.30	96.13	94.33[d]	101.02
N_O	23	23	23	6	6	6	6	6	$\Sigma_{D+T}=10$	$\Sigma_{Cat}=12$	$\Sigma_{Cat}=12$	$\Sigma_{Cat}=12$	$N_O=10$	$N_O=10$	
Na	–	–	–	0.544	0.645	0.774	0.810	0.920	0.661	0.726	2.688	2.669	0.353	0.129	0.020
Na_B	1.389	1.590	1.623	–	–	–	–	–	–	–	–	–	–	–	–
Na_A	0.866	0.558	0.571	–	–	–	–	–	–	–	–	–	–	–	–
K	0.302	0.392	0.484	–	–	–	–	–	1.901	1.798	0.132	0.264	0.075	0.870	0.954
Ca	0.611	0.410	0.377	0.424	0.308	0.191	0.111	0.148	0.433	0.493	–	0.030	0.036	0.100	–
Mg	3.031	2.147	1.992	0.182	0.147	0.072	0.064	–	0.207	0.164	–	–	0.065	0.262	1.854
Mn	0.228	0.269	0.248	0.037	0.032	0.021	0.051	–	2.651	3.487	0.578	0.456	2.234	0.395	0.011
Fe^{2+}	1.563	1.906	2.495	0.231	0.163	0.055	0.002	0.009	3.949	2.905	–	–	–	1.931	0.022
^{vi}Al	0.118	0.051	0.089	–	0.008	0.010	–	0.078	0.037	0.030	0.065	0.035	–	–	0.035
Ti	0.056	0.176	0.192	0.027	0.029	0.055	0.085	0.010	1.947	1.936	2.697	2.936	1.877	0.228	0.032
^{iv}Al	0.013	0.215	0.190	0.024	0.022	0.023	0.029	–	0.303	0.317	–	0.009	–	0.974	–
Si	7.987	7.785	7.810	1.975	1.978	1.977	1.970	2.000	7.697	7.683	4.127	3.991	4.094	2.974	3.754
Sr	–	0.065	–	–	–	–	–	–	–	0.056	1.376	0.302	–	–	–
Ba	–	–	–	–	–	–	–	–	–	–	0.095	1.141	1.735	–	–
Nb	–	–	–	–	–	–	–	–	0.016	0.034	0.029	–	0.115	–	–
Fe^{3+}	0.003	0.452	0.250	0.542	0.645	0.774	0.809	0.920	–	–	0.185	0.167	1.414	–	–
Li	–	–	–	–	–	–	–	–	–	–	–	–	–	–	1.026
mg[e]	0.66	0.48	0.42	0.19	0.15	0.08	0.07	0.0	–	–	–	–	–	–	–

(–) not detected.
[a] Total Fe given as FeO.
[b] Estimated from stoichiometry.
[c] Includes 0.60 wt.% ZnO.
[d] Includes 5.23 wt.% F; Σ_{D+T} total cations in D and T sites of astrophyllite–kupletskite structure (see Piilonen et al., 2003 for details); N_O oxygen atoms basis for calculation of structural formulae.
[e] $mg=Mg/(Fe_t+Mg)$. Compositions: (1) eckermannite entrapped by clinopyroxene, (2–3) amphibole crystal corroded and mantled by clinopyroxene, (4, 5) clinopyroxene-I, (6) clinopyroxene-II, (7) clinopyroxene-III, (8) latest prismatic aegirine associated with natrolite, (9) astrophyllite, (10) kupletskite, (11) lamprophyllite, (12) barytolamprophyllite, (13) hejtmanite rim around lamprophyllite (10), (14) biotite associated with natrolite and replacing aegirine, (15) tainiolite associated with arfvedsonite.

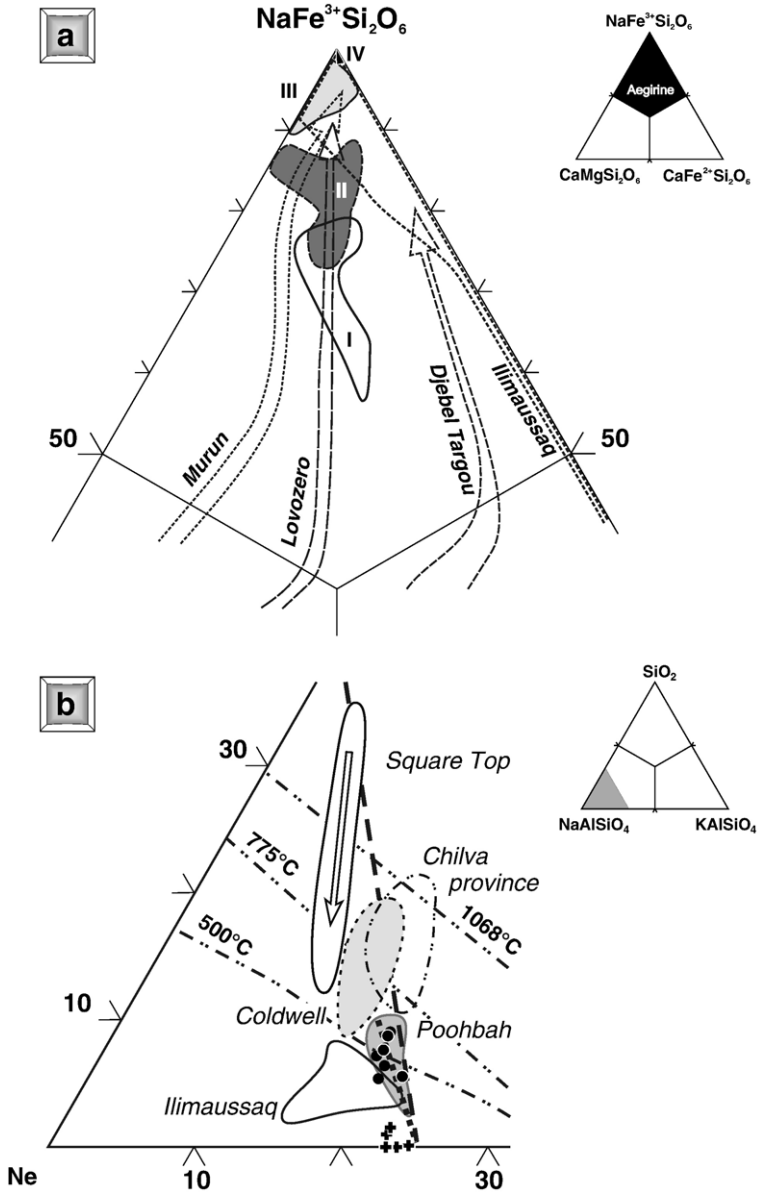

Fig. 2. Compositional variation of clinopyroxene (a) and nepheline (b). (a) Data for clinopyroxene from Murun are adopted from Mitchell and Vladykin (1996), Lovozero and Djebel Targou from Chakhmouradian and Mitchell (2002) and for Ilimaussaq from Marks and Markl (2003). Clinopyroxene generations are given in Roman numerals. (b) Compositions of the early generation of nepheline are plotted as solid circles; compositions of nepheline subjected to re-crystallization are plotted as crosses. Nepheline compositions from other occurrences are given for comparison (after Mitchell and Platt, 1979, 1982; Woolley and Platt, 1986; Wilkinson and Hensel, 1994; Coulson, 1997; Markl and Baumgartner, 2002; Marks and Markl, 2003). The dashed line ("Barth join") denotes the Dollase-Thomas compositional trend for natural nephelines (Dollase and Thomas, 1978); the dotted line denotes the Morozewicz-Buerger convergence field (Hamilton, 1961; Wilkinson and Hensel, 1994).

They represent the termination of the aegirine-enrichment trend of pyroxene compositional evolution, suggesting that the lujavrites are the most evolved rocks of the Pilansberg complex. (Note that less-evolved pyroxenes occur in other facies of the Pilansberg complex.)

4.3. Astrophyllite–kupletskite

Manganoan astrophyllite (deep orange red-to-lemon yellow pleochroism) and ferroan kupletskite (cinnamon-to-brown pleochroism) form large (0.5–2 cm) strongly

pleochroic laths in aegirine lujavrite and heterogeneous lujavrite in association with analcime and natrolite, respectively. Kupletskite is replaced by later-forming pyrophanite in the most evolved rocks. The minerals form a solid solution series with $Fe^{2+} \leftrightarrows Mn^{2+}$ substitution occurring at the sheet-forming ^{vi}[C]-sites. The $Mn/(Mn+Fe_t^{2+})$ ratio evolves from 0.4 in astrophyllite to 0.55 in kupletskite. Substitution of K by Na at the $^{x-xii}$[A]-site is less extensive (Table 1, comp. 9–10; for site designations, see Piilonen et al., 2003). In common with astrophyllite group minerals from silica-undersaturated rocks in general (Piilonen et al., 2003), Pilansberg astrophyllite–kupletskite exhibits a significant Si deficiency in the tetrahedral site positions, which is balanced by the substitution of ~0.3 afu Al^{3+}. The interlayer $^{x-xii}$[A]- and ^{x}[B]-sites are filled by Ca+Na+K+Sr. Rarely, some varieties contain significant amounts of Nb and Zr and are transitional to niobophyllite and zircophyllite.

4.4. Feldspar

Alkali feldspar is the predominant felsic mineral in the aegirine and heterogeneous lujavrites, forming euhedral-to-subhedral phenocrysts and microphenocrysts, which exhibit well-developed Carlsbad twinning together with diffuse areas of microcline twinning (Retief, 1963). The feldspar is not perthitic

Table 2
Representative compositions of some aluminosilicate minerals

	1	2	3	4	5	6	7	8	9	10	11	12	13
Na_2O	15.07	16.12	15.95	24.32	20.50	13.63	9.71	0.36	16.14	0.19	9.43	9.43	10.01
K_2O	5.95	6.17	7.88	–	–	0.07	4.99	19.36	0.11	16.70	–	–	0.12
CaO	–	–	–	0.13	3.51	0.08	0.21	0.12	–	–	–	–	–
SrO	–	–	–	–	–	–	–	–	–	–	–	8.52	15.60
BaO	–	–	–	–	–	–	–	–	–	–	23.08	10.5	0.85
Fe_2O_3 [a]	2.50	1.97	–	–	0.15	0.21	–	–	0.28	0.13	–	–	0.18
Al_2O_3	32.51	32.48	36.10	31.54	30.20	23.61	23.85	24.07	26.84	18.58	30.75	32.79	33.41
SiO_2	43.83	43.36	40.80	35.39	36.08	54.61	54.39	54.97	47.14	64.22	35.95	38.71	39.16
SO_3	–	–	–	1.28	–	–	–	–	–	–	–	–	–
Cl	–	–	–	6.95	2.19	–	–	–	–	–	–	–	–
–O≡Cl	–	–	–	1.571	0.50	–	–	–	–	–	–	–	–
Total	99.86	100.32	100.73	98.04	93.78	92.01	93.15	98.88	90.51	99.82	99.21	99.95	99.33
N_O	32	32	32	$\Sigma_{Al+Si}=12$	6	6	6	10	8	16	16	16	16
Na	5.620	6.019	5.965	7.798	6.644	0.964	0.690	0.025	1.984	0.017	2.025	1.905	1.981
K	1.460	1.516	1.939	–	–	0.003	0.233	0.896	0.009	0.989	–	–	0.016
Ca	–	–	–	0.023	0.629	0.003	0.008	0.005	–	–	–	–	–
Sr	–	–	–	–	–	–	–	–	–	–	–	0.515	0.923
Ba	–	–	–	–	–	–	–	–	–	–	1.002	0.429	0.034
Fe^{3+}	0.362	0.317	–	–	0.020	0.006	–	–	0.013	0.005	–	–	0.014
Al	7.370	7.372	8.206	6.147	6.030	1.015	1.030	1.030	2.005	1.017	4.014	4.026	4.019
Si	8.431	8.350	7.869	5.853	5.950	1.991	1.993	1.995	2.988	2.982	3.982	4.033	3.997
Σ_{Cat}	23.243	23.573	23.979	19.980	19.451	3.982	3.954	3.951	6.999	5.010	11.023	10.907	10.985
S	–	–	–	0.159	–	–	–	–	–				
Cl	–	–	–	1.948	0.620	–	–	–	–				
mol.%													
An	–	–	–			0.29	0.38	0.62	–				
Fe–Ne [b]	–	4.02	–			0.29	–	–	0.41				
Kls	18.83	18.11	24.59			0.15	11.22	67.32	0.29				
Ne	72.47	72.65	75.63			46.99	33.25	1.71	59.03				
Qtz	8.70	5.22	0.22			52.28	55.15	30.36	40.27				

(–) not detected.
N_O oxygen atoms basis for calculation of structural formulae. Compositions: (1–3) nepheline: (1) core and (2) periphery of a chadacryst preserved in clinopyroxene, (3) relicts of nepheline cemented by analcime; (4) sodalite chadacryst preserved in eudialyte-I; (5) altered sodalite in contact with analcime; (6) analcime replacing nepheline; (7) analcime replacing microcline; (8) leucite formed by the breakdown of microcline and cemented by analcime; (9) natrolite replacing nepheline, analcime and sodalite; (10) microcline; (11–13) banalsite–stronalsite solid solution: (11) banalsite core, (12) intermediate areas, (13) stronalsite margins.
[a] Calculated from stoichiometry.
[b] Theoretical $(Na,K)Fe^{3+}SiO_4$ end-member.

and typically contains less than 1.5 wt.% Na_2O (Table 2, comp. 10). X-ray diffraction demonstrates that the mineral is fully ordered triclinic microcline. During deuteric alteration, the alkali feldspar can be replaced by aegirine, sodalite, analcime, natrolite and rarely by leucite plus analcime.

Albite appears to be absent as a primary phase from aegirine and heterogeneous lujavrite. Flow-aligned prismatic crystals of pure albite with polysynthetic twinning were recognized only in melanolujavrite. Small crystals of pure albite also occur as inclusions in euhedral nepheline phenocrysts in this rock. Albite can be replaced by analcime and natrolite. Both alkali feldspar and albite occur in some of the pseudomorphs after eudialyte in melanolujavrite.

4.5. Nepheline

Fresh nepheline occurs as inclusions in unaltered poikilitic crystals of clinopyroxene-I and eudialyte in heterogeneous lujavrites (Fig. 1e,g), whereas nepheline in contact with analcime and natrolite is corroded and pseudomorphed (Fig. 1a,b). Nepheline forms euhedral phenocrysts in aegirine lujavrite and melanolujavrite. The least-altered nepheline (Ne-I) has the composition $Ne_{72.5}Ks_{18.8}Qtz_{8.7}$ (wt.%) and contains 2.5 wt.% Fe_2O_3. With replacement by sodalite and zeolites, the Qtz content decreases to 5 wt.% coupled with decreasing Fe contents (Table 2, comp. 1–2). All compositions fall in the Morozewicz-Buerger convergence field for plutonic nepheline (Fig. 2b), suggesting equilibration temperatures of 580–600 °C. Altered and corroded nepheline in immediate contact with analcime and natrolite (Ne-II) approaches the stoichiometric composition (Table 2, comp. 3; Fig. 2b), demonstrating that significant cation exchange and re-equilibration with sodium-rich deuteric fluids has occurred.

4.6. Sodalite

Sodalite occurs as translucent violet grains of 4–6 mm in size in melanolujavrite or partial-to-complete pseudomorphs after nepheline crystals in heterogeneous lujavrite (Fig. 1e). Its abundance varies sympathetically with that of eudialyte, being 20–25 vol.% in melanolujavrite and low-to-absent in heterogeneous lujavrite. The sodalite is represented by a S-rich variety and contains ~1.3 wt.% SO_3 (Table 2, comp. 4). Upon deuteric alteration, sodalite releases Cl, S and some Na (Table 2, comp. 5), and is initially replaced by analcime and subsequently by natrolite.

4.7. Apatite

Apatite is a common accessory phase which shows wide variations in composition from primary fluorapatite to strontium-apatite and ultimately to Si-rich belovite-(Ce) and strontian britholite.

5. Secondary minerals formed by deuteric/hydrothermal processes

5.1. Analcime

Analcime hosts the most sodic parageneses, corroding and replacing primary nepheline (Fig. 1b), sodalite, eudialyte and alkali feldspar (Fig. 1d). The mineral occurs as turbid grains and reaction rims. Analcime formed after nepheline and/or sodalite has a stoichiometric composition (Table 2, comp. 6), whereas analcime replacing microcline contains ~5 wt.% K_2O (Table 2, comp. 7). This unusual potassian analcime is armoured by a grid of leucite lamellae, which have an interlocking "chess-board" morphology. The leucite is K-deficient and contains only minor Na and Ca (Table 2, comp. 8).

5.2. Natrolite

Natrolite, which corrodes and replaces all precursor Na–Al silicates (Fig. 1b), is the latest aluminosilicate to crystallize. The mineral occurs as colourless, columnar reaction rims or massive aggregates and approaches stoichiometric composition (Table 2, comp. 9).

5.3. Deuteric Na–Zr-silicates

An unidentified deuteric Na–Zr-silicate phase is abundant among the breakdown products of eudialyte-I and -II (see below) and occurs as fine-grained aggregates or rims around zircon and eudialyte-I and -II. The size of the crystals and intimate intergrowths with other minerals (Fig. 3a–h) precludes identification by optical or X-ray diffraction methods. By analogy with similar subsolidus alteration of eudialyte in Ilímaussaq lujavrite (Rose-Hansen and Sørensen, 2002), we consider the mineral most probably belongs to the catapleiite group. The mineral shows considerable inter-grain compositional variation from the Na-dominant end-member to calcian varieties replacing eudialyte-II and containing up to 4.5 wt.% SrO (Table 3, comp. 5 and 6). In the hyperagpaitic assemblage replacing eudialyte (see below), uniaxial negative

hilairite (Table 3, comp. 7) occurs as rosettes of platy euhedral crystals (Fig. 3d). In lujavrite, tiny plates of a paraumbite-like mineral (Table 3, comp. 9) occur in analcime formed after alkali feldspar.

5.4. Other minerals

Numerous exotic sub-microscopic minerals occur in the postmagmatic parageneses. These are commonly either too small to analyse accurately or decompose rapidly under the electron beam. Apart from using some of these minerals as indicators of the miaskitic, agpaitic or hyperagpaitic character of the deuteric parageneses (Khomyakov, 1995), description of their composition and genesis is beyond the scope of this paper. Minerals recognized to date are: allanite-(Ce) (Table 3, comp. 15), allanite-(La) (Table 3, comp. 16), banalsite–stronalsite solid solution series (Table 2, comp. 11–13), barytolamprophyllite (Table 1, comp. 12), betafite, belovite-(Ce), britholite, burbankite, delindeite, ecandrewsite–pyrophanite solid solution series (Mitchell and Liferovich, 2004), hejtmanite (Table 1, comp. 13), huttonite, britholite-(Ce), light-REE arsenates and phosphoarsenates (gasparite, retzian, etc.), rare earth carbonates [including ancylite-(Ce), ancylite-(La), bastnäsite-(Ce), bastnäsite-(La)], hollandite-like oxides, lamprophyllite (Table 1, comp. 11), olekminskite, paraumbite (Table 3, comp. 3), pectolite–serandite, rengeite (Table 3, comp. 10), a fluoro-analog of strontium-apatite, strontianite, strontiopyrochlore (Table 3, comp. 12), Zr–Nb-bearing titanite (Table 3, comp. 11), thorite, U–Si–Pb-bearing pyrochlore, a wöhlerite-like mineral (Table 3, comp. 14), an unidentified Ca–Sr–Y–Zr oxide (Table 3, comp. 13) and an unknown Sr–Zr silicate phase, a possible analog of komkovite (Table 3, comp. 8). In the hyperagpaitic replacement assemblages, two Na–Al-bearing phases have been recognized as 1–15 μm grains; importantly, these have the Si:Al ratios of ussingite and naujakasite, i.e. sodic aluminosilicates that are typomorphic minerals of hyperagpaitic rocks (Khomyakov et al., 2001).

6. Eudialyte parageneses and alteration

On the basis of textural relationships, we have recognized three varieties of eudialyte in the lujavrites. *Eudialyte-I* is a late magmatic phase forming poikilitic grains (0.1–2.5 cm) enclosing euhedral chadacrysts of clinopyroxene, amphibole, nepheline (and/or) sodalite and microcline (Fig. 1c,e). Fresh material occurs only in a few samples of heterogeneous lujavrite and, in other varieties, it is typically altered and replaced by a complex fine-grained assemblage of zircon, pyrochlore, fergusonite, britholite, allanite, NZS-phase(s), K-feldspar, albite and zeolites.

Eudialyte-II occurs in complex pseudomorphs after abundant small (0.05–2.0 mm) euhedral phenocrysts. The pseudomorphs consist of the same mineral assemblage as described above replacing eudialyte-I. Relicts of original primary eudialyte-I (Fig. 1d) occur in some of the pseudomorphed grains indicating that the phenocrysts were originally composed of eudialyte-I. Eudialyte-II is more evolved in terms of its composition than eudialyte-I (see below) and thus must represent a later generation of eudialyte; hence, the designation as eudialyte-II.

Eudialyte-III occurs as a late stage subsolidus alteration phase that commonly replaces and mantles all precursor eudialyte and other zirconium silicates. On the basis of textural relationships, it is interpreted to be of hydrothermal origin.

Three styles of replacement of eudialyte have been recognized.

Type 1, involves decomposition and replacement by complex aggregates of zircon, fergusonite, allanite, britholite, titanite, pyrochlore, albite and potassium feldspar. This assemblage is referred to here as a "miaskitic" paragenesis, using Khomyakov's (1995) terminological scheme. Relict fragments of eudialyte-I and -II can be found in this paragenesis.

Type 2 replacement consists of pseudomorphing by complex aggregates dominated by deuteric Na–Zr-silicate(s), analcime, serandite–pectolite, strontium apatite, stronalsite, lamprophyllite and numerous sodic microphases replacing both eudialyte-II and the miaskitic paragenesis. This highly sodic assemblage is referred to here as an "agpaitic-to-hyperagpaitic" paragenesis, using Khomyakov's (1995) terminological scheme. Zircon and other minerals characteristic of the miaskitic paragenesis, when present, are not in equilibrium with the deuteric Na–Zr-silicates as shown by corrosion and replacement textures (Fig. 3a–c). Hilairite (Fig. 3d) forms during the later stages of alteration.

Type 3 replacement involves mantling of any residual eudialyte and zircon, and replacement of deuteric Na–Zr-silicate by strongly pleochroic eudialyte-III (Fig. 3e–g) together with barytolamprophyllite as late hydrothermal phases.

All of the alteration styles are considered to have occurred under subsolidus conditions by interaction of pre-existing eudialyte and other minerals with deuteric sodium- and chlorine-bearing aqueous fluids. We have observed that eudialyte-I and -II can alter in sequence from type 1 through type 2 to type 3 assemblages or

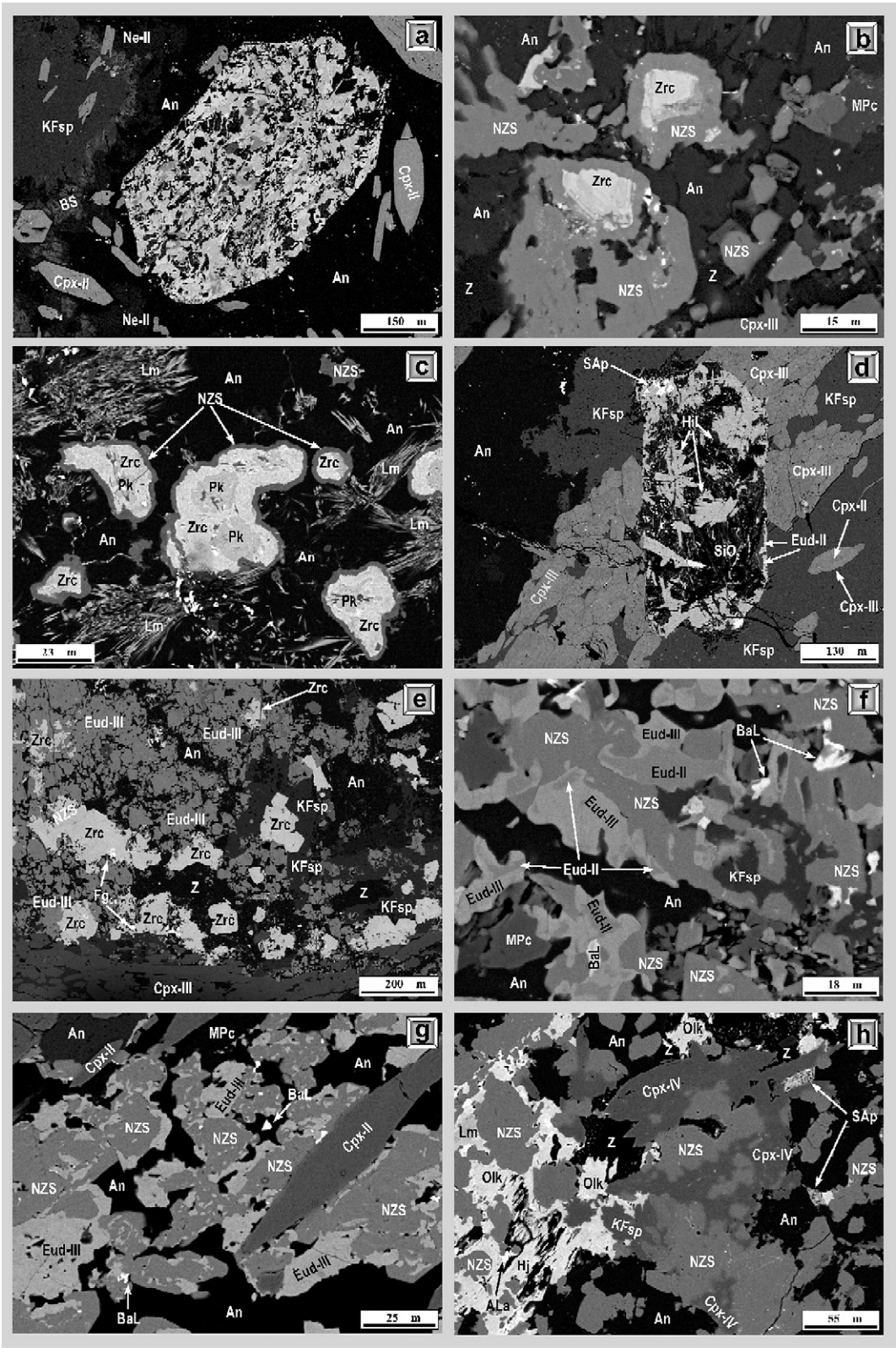
a
Ne-II
An
KFsp
BS
Cpx-II
Cpx-II
An
Ne-II
150 m
b
An
An
Zrc
MPc
NZS
NZS
Zrc
An
An
NZS
Z
Z
NZS
Cpx-III
15 m
c
Lm
An
NZS
NZS
An
Zrc
Zrc
Lm
Pk
Pk
Zrc
Pk
Lm
An
An
Zrc
Pk
Lm
Zrc
23 m
d
SAp
Cpx-III
KFsp
KFsp
Hl
An
Cpx-III
Cpx-II
Eud-II
SiO2
Cpx-III
Cpx-III
KFsp
130 m
e
Zrc
Eud-III
Zrc
Eud-III
An
An
KFsp
NZS
Eud-III
Zrc
Zrc
Zrc
KFsp
Z
Fg
Eud-III
Zrc
Zrc
Zrc
Z
KFsp
Cpx-III
200 m
f
NZS
NZS
Eud-III
BaL
Eud-II
NZS
Eud-III
Eud-II
KFsp
NZS
Eud-III
Eud-II
An
MPc
BaL
NZS
NZS
An
18 m
g
An
MPc
Cpx-II
An
Eud-III
BaL
NZS
NZS
Cpx-II
NZS
NZS
An
NZS
Eud-III
Eud-III
BaL
An
25 m
h
An
Olk
Z
Z
Cpx-IV
SAp
Lm
NZS
Z
NZS
Cpx-IV
NZS
Olk
Olk
KFsp
An
NZS
Hl
NZS
ALa
An
Cpx-IV
85 m

apparently directly to the types 2 and 3 assemblages. It is of course possible that a type 1 paragenesis has in some instances been completely replaced by the type 2 assemblage. Regardless, the evolution of the replacement products is from an orthomagmatic agpaitic paragenesis (astrophyllite, eudialyte-I, rinkite, etc.) followed by an early miaskitic paragenesis (zircon, early britholite, allanite, fergusonite and pyrochlore) through an agpaitic (eudialyte-II, lamprophyllite) and hyperagpaitic paragenesis (NZS, ussingite, stronalsite, analcime), and ultimately back to a late agpaitic mineral assemblage (eudialyte-III, barytolamprophyllite) followed by a later miaskitic paragenesis (late allanite, britholite, titanite and pyrochlore), reflecting changes in the alkalinity of the deuteric/hydrothermal fluids. Further alteration and replacement always results in the superposition of natrolite, hejtmanite, allanite and diverse Ba- and Mn-based minerals onto the types 2 and 3 assemblages, and ultimately to the deposition of allanite-(La), La-dominant carbonates of REE and in places culminates with the formation of a mineral with the composition of SiO_2 (polymorph unidentified; Fig. 3d).

7. Eudialyte composition

Classification of the eudialyte group minerals on the basis of microprobe data is not straightforward (Johnsen and Grice, 1999), and further characterization according to the nomenclature of the eudialyte group developed by Johnsen et al. (2003a) on the basis of calculated empirical formulae is to a certain extent arbitrary. Following Johnsen and Grice (1999), our data (127 compositions) and all comparative data are classified on the basis of structural formulae calculated with $\Sigma_{(Si+Al+Zr+Ti+Hf+Nb)}=29$ afu.

Compositions of Pilansberg eudialyte are very variable in terms of Sr, REE, Ca, Nb, Zr, Mn, Fe and (Na+K), and less so in Zr, with low abundances of Al, K, Ba and Y (Table 4). Mg, Ta, W, heavy lanthanides and P are below detection limits. Eudialyte in contact with natrolite and associated low-temperature minerals is always depleted in (Na+Cl) (Table 4, comp. 4) or completely decomposed into a fine-grained intimate mixture of hydrosilicates and oxides. Thus, Na and Cl are inferred to have been leached from the eudialyte during the low-temperature natrolite stage of alteration. The compositions of eudialyte subjected to such alteration are not considered further here.

Eudialyte-I, considered as being the least-evolved relict variety in terms of Mn and Nb content, is compositionally homogeneous (Fig. 1e). The least-altered grains demonstrate the highest abundances of Na and Cl (11.1–11.9 and ~1.9 wt.%, respectively) contain 3.9–4.2 wt.% SrO and 0.6–1.7 wt.% TiO_2 and concentrations of Nb, Mn and Fe (Table 4, comp. 1–2) close to those of eudialyte sensu lato (Johnsen and Grice, 1999). In terms of the calculated occupancy of the *M*(3) and *M*(2) sites (Fig. 4a), some examples of eudialyte-I are Mn-dominant and represent a Mn-analog of Nb-poor eudialyte, i.e. manganoan eudialyte. These are more manganoan than eudialyte group minerals from the Gardiner, Ilímaussaq and Lovozero peralkaline massifs but comparable to counterparts from the Burpala complex and the Saint-Amable sill (Fig. 4 and references therein). Similar eudialyte occurs in some Mont Saint-Hilaire rocks and in Poços de Caldas lujavrite (Fig. 4a).

The relict phase, termed eudialyte-II, recognized by its relatively low average atomic number in back-scattered electron images (Fig. 3f), has the most variable composition. Texturally different lujavrites contain eudialyte-II of different composition. In addition, its composition varies within any given sample although individual grains are homogeneous. In general, eudialyte-II in lujavrite and melanolujavrite defines relatively limited but different compositional fields. These are overlapped by the large diffuse field of compositions observed for eudialyte-II in the inequigranular and porphyritic lujavrite (Figs. 4a and 5). In terms of occupancy of the *M*(3) and *M*(2) sites (Fig. 4a), eudialyte-II in lujavrite is close to or slightly more niobian–manganoan than eudialyte-I and might be interpreted as transitional from eudialyte to kentbrooksite.

Fig. 3. Back-scattered electron images illustrating some characteristic textures involving eudialyte in the Pilansberg lujavrites. (a) Altered crystal of euhedral eudialyte-II (?) replaced by zircon-free "hyperagpaitic" mineral assemblage; (b) corrosion and replacement of zircon; (c) substitution of a primary parakeldyshite-like phase by zircon and zircon by NZS phase(s); (d) hilairite and a silica phase replacing a decomposed eudialyte-II crystals; (e) zircon-bearing mineral assemblage formed by alteration of eudialyte-I with zircon followed by the NZS phase(s) and then by the latest hydrothermal eudialyte-III; (f) eudialyte-III replacing both eudialyte-II and the NZS phase(s); (g) replacement of the NZS phase(s) by late eudialyte; (h) corrosion and replacement of the NZS phase(s) by the latest-forming aegirine, lamprophyllite group minerals and olekminskite. Mineral generations are given in Roman numerals: ALa=ancylite-(La), An=analcime, BaL=barytolamprophyllite, Cpx=clinopyroxene, Eud=eudialyte, FgCe=fergusonite-(Ce), Hil=hilairite, Hj=hejtmanite, KFsp=potassic feldspar, Lm=lamprophyllite, MPc=manganoan pectolite, Ne=nepheline, NZS=an unidentified catapleiite-like deuteric Na–Zr-silicate(s), Olk=olekminskite, Pk=parakeldyshite-like sodic zirconosilicate, SAp=strontium-apatite, SiO_2=a fibrous silica phase, Z=natrolite, Zrc=zircon.

Table 3
Representative compositions of zirconium minerals and other phases

	1	2	3	4	5	6	7	8	9	10	11	12	13	14	15	16
Na_2O	8.92	4.24	–	0.88	9.17	15.07	6.08	3.73	–	–	0.79	5.90	0.67	10.44	0.30	0.98
K_2O	–	–	–	–	–	–	1.33	0.33	6.00	–	0.41	–	–	0.16	–	–
CaO	26.05	0.57	–	1.24	4.18	–	3.45	2.38	3.01	0.67	22.92	15.83	27.57	6.32	8.30	8.60
SrO	0.26	–	–	–	–	–	0.21	15.06	–	34.32	–	4.52	27.66	5.67	2.59	3.58
BaO	–	–	–	–	–	0.16	–	–	10.21	–	–	–	–	–	–	–
MnO	1.78	0.12	–	0.29	–	–	0.17	–	–	0.015	0.27	0.47	–	–	4.17	2.88
FeO[a]	0.42	0.1	–	0.69	0.47	0.47	1.25	0.78	–	0.89	0.91	–	–	0.53	13.58	15.43
La_2O_3	–	–	–	–	–	–	–	–	–	–	–	0.18	2.28	–	11.38	10.95
Ce_2O_3	–	–	0.24	–	–	–	–	–	–	0.87	–	–	2.12	–	12.78	6.87
Y_2O_3	0.30	–	–	–	–	–	–	–	–	–	–	–	15.02	–	–	–
Al_2O_3	–	–	–	1.06	–	–	–	–	–	–	0.23	–	–	–	7.54	9.49
TiO_2	10.46	–	–	–	–	–	0.45	–	2.75	27.54	29.88	8.57	–	3.45	6.61	2.38
Nb_2O_5	0.92	0.68	0.25	0.44	–	0.52	1.68	1.33	–	0.30	6.84	52.32	–	32.02	0.60	0.45
ZrO_2	13.26	51.02	65.79	58.81	31.79	30.69	30.27	28.67	22.12	11.97	6.24	3.00	25.29	14.50	–	3.70
HfO_2	0.60	0.79	1.48	0.78	0.61	–	0.54	0.46	–	–	–	–	–	–	–	–
SiO_2	33.96	36.82	32.15	28.15	44.19	44.93	43.99	40.16	40.91	22.38	30.65	9.00	–	25.15	30.80	31.73
F	5.17	–	–	–	–	–	–	–	–	–	–	4.56	–	4.26	–	–
–O≡F	2.18	–	–	–	–	–	–	–	–	–	–	1.92	–	1.79	–	–
Total	99.92	94.34	99.80	92.97	90.54	91.37	89.42	92.90	85.25	99.09	98.37	97.87	100.50	100.71	98.65	97.88[b]
$^{St}B_{Calc}$	$\Sigma_C=3$[c]	$N_O=7$	$N_O=4$	$N_O=4$	$N_O=9$	$N_O=9$	$N_O=9$	$N_O=9$	$N_O=18$	$N_O=22$	$N_{cat}=3$	$\Sigma_B=3$[c]	–	$\Sigma_C=3$[d]	$N_O=12$	$N_O=12$
Na	1.061	0.444	–	0.057	1.198	1.947	0.803	0.517	–	–	0.081	0.564		1.232	0.056	0.186
Ca	2.084	0.033	–	0.044	0.302	–	0.252	0.182	0.486	0.131	0.851	0.836		0.412	0.855	0.903
Sr	0.009	–	–	–	–	–	0.008	0.625	–	3.644	–	0.129		0.200	0.144	0.203
Ba	–	–	–	–	–	0.004	–	–	0.605	–	–	–		–	–	–
Mn	0.093	0.005	–	0.008	–	–	0.010	–	–	0.023	0.008	0.020		–	0.339	0.239
Fe^{2+}	0.022	0.005	–	0.019	0.026	–	0.071	0.047	–	0.136	0.024	–		0.027	1.091	1.264
K	–	–	–	–	–	–	0.116	0.030	1.158	–	–	–		0.012	–	–
La	–	–	–	–	–	–	–	–	–	–	–	0.003		–	0.403	0.396
Ce	–	–	0.003	–	–	–	–	–	–	0.058	–	–		–	0.450	0.246
Y	0.010	–	–	–	–	–	–	–	–	–	–	–		–	–	–
Al	–	–	–	0.042	–	–	–	–	–	–	0.005	–		–	0.854	1.096
Ti	0.483	–	–	–	–	–	0.023	–	0.313	3.792	0.779	0.318		0.158	0.478	0.175
Nb	0.023	0.017	0.003	0.007	–	0.016	0.052	0.043	–	0.025	0.107	1.166		0.881	0.026	0.020
Zr	0.397	1.345	0.991	0.960	1.045	0.997	1.005	1.000	1.632	1.069	0.105	0.072		0.430	–	0.176
Hf	0.011	0.012	0.010	0.007	0.012	–	0.010	0.009	–	–	–	–		–	–	–
Si	2.084	1.990	0.993	0.942	2.978	2.994	2.996	2.873	6.190	4.097	1.036	0.444		1.531	2.960	3.109
F	1.004	–	–	–	–	–	–	–	–	–	–	0.711		0.820	–	–

(–) not detected.
$^{St}B_{Calc}$ basis for calculation of structural formulae.
Compositions: (1) rosenbushite in paragenesis with magnesio-arfvedsonite (altered); (2) an unidentified sodic zirconosilicate from hyperagpaitic paragenesis; (3) euhedral zircon in altered eudialyte-I aggregate; (4) zircon (?) subjected to alteration and replacement by catapleiite-like Na–Zr-silicate phase; (5) an unidentified Na–Zr-silicate phase replacing eudialyte-II and entrapped in late clinopyroxene; (6) an Na–Zr-silicate phase replaced by eudialyte-III; (7) hilairite associated with zincian pyrophanite and analcime; (8) an unidentified phase entrapped in catapleiite-like Na–Zr-silicate phase; (9) a paraumbite-like phase (note: the analysis is performed on a badly polished surface); (10) a rengeite associated with stronalsite; (11) late titanite as an eudialyte alteration product, (12) pyrochlore among products of alteration of eudialyte; (13) an unidentified Ca–Sr–Y–Zr phase; (14) a whölerite-like phase associated with an unidentified Na–Zr-silicate phase(s) replacing eudialyte-II; (15) allanite-(Ce), (16) allanite-(La).
[a] Total Fe given as FeO.
[b] Includes 0.84 wt.% Nd_2O_3.
[c] Σ_B sum of B-site cations.
[d] $\Sigma_C=\Sigma_{(Si+Ti+Nb+Zr+Hf)}$.

Eudialyte-II in lujavrite is relatively poor in REE and contains 4–4.3 wt.% SrO (Table 4, comp. 7–8; Fig. 5).

Eudialyte-II in melanolujavrite has a Nb–Mn-rich composition (Table 4, comp. 9–10; Figs. 4 and 5). It contains up to (wt.%) 3.9 Nb_2O_5, 8.5 MnO_2, 1.3–3.5 SrO and 0.8–4.1 REE_2O_3 with La>Ce, and is interpreted as kentbrooksite in terms of cationic composition. The content of Sr in eudialyte-II in melanolujavrite correlates positively with (Mn+Nb) and the proportion of the "kentbrooksite molecule" (Johnsen and Grice, 1999).

Table 4
Representative compositions of eudialyte in Pilansberg lujavrite

	Anhedral poikilitic eudialyte-I						Euhedral eudialyte-II					Hydrothermal eudialyte-III					
	1	2	3	4	5	6	7	8	9	10	11	12	13	14	15	16	17
Na_2O	11.92	11.13	9.36	6.16	11.28	10.62	9.50	8.67	9.94	9.21	10.83	7.51	7.30	9.39	9.41	10.24	6.68
K_2O	–	0.18	0.41	0.82	0.24	–	0.69	0.69	0.24	0.18	0.27	0.85	0.86	0.52	0.43	0.39	–
CaO	10.18	11.73	10.31	9.86	12.98	11.55	12.33	11.07	12.17	9.65	9.63	10.88	10.88	9.48	9.22	9.44	8.56
SrO	3.94	4.21	5.50	5.74	0.26	1.11	4.33	5.81	1.32	3.46	5.06	7.31	7.19	1.05	0.66	5.96	2.08
BaO	–	0.96	0.67	0.42	–	–	–	0.32	0.20	–	–	–	–	–	–	0.45	–
MnO	4.15	4.14	3.83	4.45	2.93	5.47	2.63	4.54	8.46	6.96	3.93	6.39	4.99	7.45	7.91	6.67	10.07
FeO_t[a]	3.95	3.06	2.75	1.78	3.92	1.71	4.12	3.09	0.15	0.31	3.0	1.49	2.38	0.21	0.31	0.33	0.84
Ce_2O_3	0.50	0.20	–	–	0.90	3.49	0.48	–	0.75	2.34	0.50	–	0.47	3.45	5.43	1.35	2.93
La_2O_3	–	–	–	–	0.50	2.56	0.23	–	0.36	1.68	–	–	0.25	4.06	3.03	1.90	3.06
Nd_2O_3	–	–	–	–	–	0.58	–	–	–	–	–	–	–	–	0.55	–	1.17
Y_2O_3	–	–	–	–	–		–	–	0.32	–	–	–	–	0.69	–	–	–
Al_2O_3	–	0.41	0.28	–	–	–	–	–	–	–	–	–	–	–	–	–	–
TiO_2	1.07	0.62	0.32	–	0.12	–	0.35	0.41	–	–	0.57	–	–	–	–	–	–
Nb_2O_5	0.82	0.71	1.22	4.02	1.32	4.01	1.81	1.92	3.83	3.78	1.88	4.19	4.20	4.17	3.81	4.17	3.41
ZrO_2	12.02	11.64	12.21	11.66	12.59	11.17	12.04	11.91	11.51	11.72	11.69	12.41	12.75	11.62	10.89	11.09	11.51
HfO_2	0.29	0.29	0.29	0.25	–	–	0.27	0.32	–	0.31	0.35	–	0.39	0.32	0.22	–	0.21
SiO_2	48.48	48.02	49.01	46.31	49.06	45.66	49.41	48.68	47.65	45.57	47.47	46.11	46.12	45.89	45.87	45.90	44.20
Cl	1.91	1.88	1.84	0.89	1.28	1.59	1.93	1.09	1.44	1.42	1.50	1.17	1.21	0.60	0.32	1.26	0.34
–O≡Cl	0.43	0.42	0.42	0.20	0.29	0.36	0.44	0.25	0.32	0.32	0.34	0.26	0.27	0.14	0.07	0.35	0.08
Total	98.80	98.76	97.58	92.16	97.09	99.16	99.68	98.27	98.06	96.27	96.34	98.35	98.76	99.81	97.99	99.55	94.98
Na	12.055	11.368	9.370	6.428	11.347	11.281	9.464	8.743	10.156	9.756	11.163	7.769	7.553	9.863	9.990	10.824	7.304
K	–	0.121	0.270	0.563	0.159	–	0.452	0.458	0.161	0.125	0.183	0.579	0.585	0.359	0.300	0.271	–
Ca	5.689	6.621	5.703	5.686	7.215	6.780	6.788	6.169	6.871	5.649	5.485	6.219	6.220	5.502	5.409	5.514	5.172
Sr	1.192	1.286	1.647	1.791	0.078	0.353	1.290	1.752	0.403	1.096	1.560	2.261	2.225	0.330	0.210	1.884	0.680
Ba	–	0.198	0.136	0.089	–	–	–	0.065	0.041	–	–	–	–	–	–	0.096	–
Mn	1.833	1.847	1.675	2.029	1.288	2.538	1.145	2.000	3.776	3.221	1.770	2.888	2.255	3.418	3.668	3.080	4.810
Fe_t^{2+}	1.723	1.348	1.187	0.801	1.701	0.784	1.770	1.344	0.066	0.142	1.334	0.665	1.062	0.095	0.142	0.150	0.396
Ce	0.095	0.039	–	–	0.171	0.700	0.090	–	0.145	0.468	0.997	–	0.092	0.892	1.088	0.269	0.605
La	–	–	–	–	0.096	0.517	0.044	–	0.070	0.339	–	–	0.049	0.811	0.612	0.382	0.636
Nd	–	–	–	–	–	0.113	–	–	–	–	–	–	–	–	0.108	–	0.236
Y	–	–	–	–	–	–	–	–	0.081	–	–	–	–	0.199	–	–	–
Al	–	0.255	0.170	–	–	–	–	–	–	–	–	–	–	–	–	–	–
Ti	0.420	0.246	0.124	–	0.047	–	0.135	0.160	–	–	0.228	–	–	–	–	–	–
Nb	0.193	0.169	0.285	0.978	0.310	0.993	0.420	0.451	0.912	0.934	0.452	1.011	1.013	1.021	0.943	1.028	0.869
Zr	3.057	2.990	3.074	3.060	3.185	2.984	3.017	3.021	2.978	3.122	3.031	3.229	3.318	3.070	2.908	2.948	3.165
Hf	0.043	0.044	0.043	0.038	–	–	0.040	0.048	–	0.048	0.053	–	0.059	0.049	0.034	–	0.034
Si	25.287	25.297	25.304	24.923	25.453	25.017	25.388	25.320	25.109	24.896	25.237	24.761	24.610	24.860	25.115	25.024	24.926
Cl	1.688	1.678	1.610	0.812	1.125	1.476	1.680	1.315	1.286	1.315	1.351	1.058	1.094	0.551	0.297	1.164	0.325
$\Sigma_{CATIONS}$	51.587	51.829	48.988	46.386	51.05	52.06	50.043	49.531	50.769	49.796	51.493	49.382	49.011	50.469	50.527	51.470	48.833

Structural formulae calculated on the basis of $\Sigma_{(Si+Al+Zr+Ti+Hf+Nb)}=29$ (see Johnsen and Grice, 1999 for details).
(–) not detected.
Compositions: (1–2) anhedral poikilitic eudialyte in heterogeneous lujavrite, core and margin, respectively; (3–4) eudialyte subjected to low-temperature alteration in contact with latest zeolite-forming hydrothermal solutions (natrolite stage); (5–6) anhedral eudialyte in white foyaite, core and a margin, respectively; (7–8) eudialyte-II lujavrite; (9–10) eudialyte-II in melanolujavrite; (11) eudialyte-II in heterogeneous lujavrite; (12–13) eudialyte-III in lujavrite; (14–15) eudialyte in melanolujavrite where 15 accounts for outermost (latest) area; (16) eudialyte-III in heterogeneous lujavrite; (17) eudialyte in Ledig foyaite.
[a] Total Fe given as FeO_t.

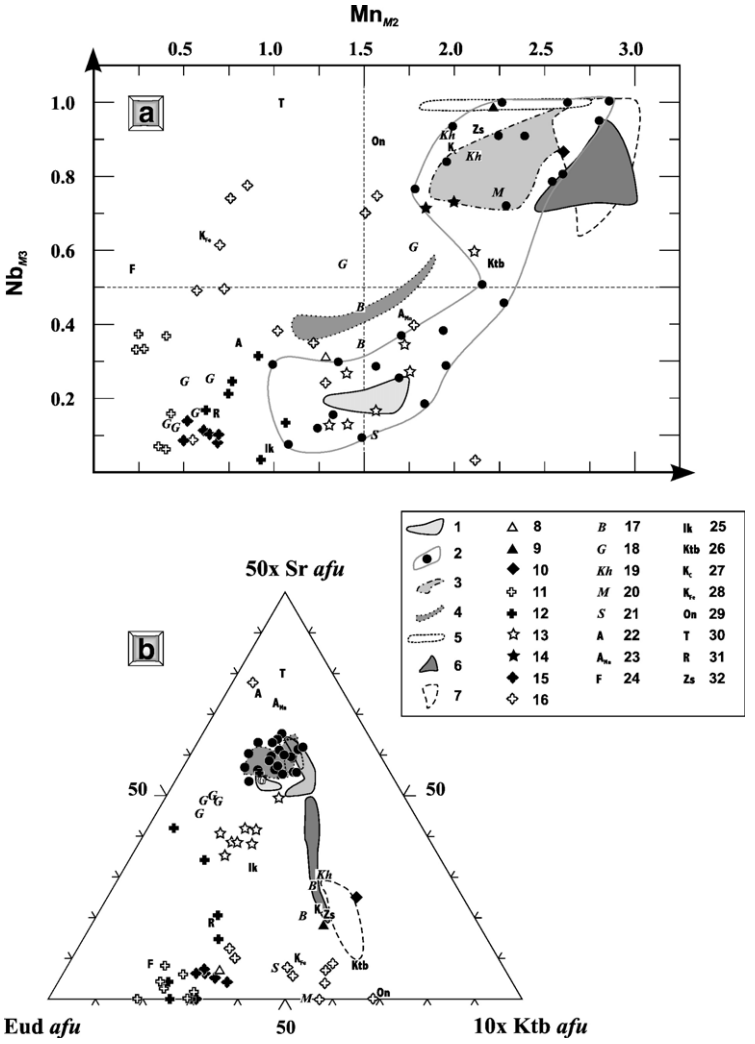

Fig. 4. Compositional variations of eudialyte (a) in terms of Nb in the *M*(3) versus Mn in the *M*(2) sites calculated following the procedure of Johnsen and Grice (1999) and (b) in terms of Sr versus "Eud" (eudialyte) and "Ktb" (kenbrooksite), with two latter components calculated as [(Si,Al)+Ca +Fe_t] and [(Nb, other *M*(3) elements)+REE+Mn] following the procedure of Johnsen and Grice (1999); the multiplier factors for parameters plotted are arbitrary. (1–10) Eudialyte in Pilansberg rocks, including: inequigranular and porphyritic lujavrites: (1) eudialyte-I, (2) eudialyte-II, (3) eudialyte-III; lujavrite: (4) eudialyte-II and (5) eudialyte-III; melanolujavrite: (6) eudialyte-II and (7) eudialyte-III; white foyaite: (8) eudialyte-I and (9) eudialyte-II; (10) eudialyte in Ledig foyaite, unspecified. (11–14) Eudialyte in lujavrite from other localities: (11) Ilímaussaq, (12) Lovozero; Poços de Caldas: (13) eudailyte-I and (14) eudialyte-II. (15–21) Eudialyte from other peralkaline complexes: (15) Kipawa, (16) Mont Saint-Hilaire, (17) Burpala, (18) Gardiner, (19) Khibina, (20) Ilomba, Malawi, (21) Saint-Amable sill. (22–32) Eudialyte-group minerals (holotypes): (22) khomyakovite, (23) manganokhomyakovite, (24) feklichevite, (25) ikranite, (26) kentbrooksite, (27) carbokentbrooksite, (28) ferrokentbrooksite, (29) oneillite, (30) taseqite, (31) raslakite, (32) zirsilite-(Ce). Note that real site occupancies, especially for transitional compositions, may differ from those calculated and plotted here due to: site vacancies, structural defects and the presence of unaccounted elements (Johnsen and Grice, 1999). Compositions of eudialyte family minerals from other occurrences are recalculated in the same manner (after Bussen and Sakharov, 1972; Coulson, 1997; Johnsen et al., 1998, Johnsen and Grice, 1999; Pekov et al., 2001; Chukanov et al., 2003; Johnsen et al., 2003a, 2003b; Kohmyakov et al., 2003; Kostyleva-Labuntsova et al., 1978; Petersen et al., 2004).

Conspicuous linear trends of composition are evident in plots of [Eud–50Sr–10Ktb] (Fig. 4b).

The composition of eudialyte-II in the heterogeneous lujavrite (Table 4, comp. 11) is the most variable in terms of Nb and Mn, and ranges from compositions similar to those of Nb–Mn-poor eudialyte-I to compositions with the *M*(3) and *M*(2) positions filled only by Nb and Mn, respectively (Fig. 4a). The abundance of Sr ranges from 1.3 to 4.7 wt.% SrO and REE_2O_3 from not detectable to 1.6 wt.% with Ce>La. Our data suggest that most of samples of eudialyte-II in the heterogeneous lujavrite have more Nb and Mn at the *M*(3) and *M*(2)

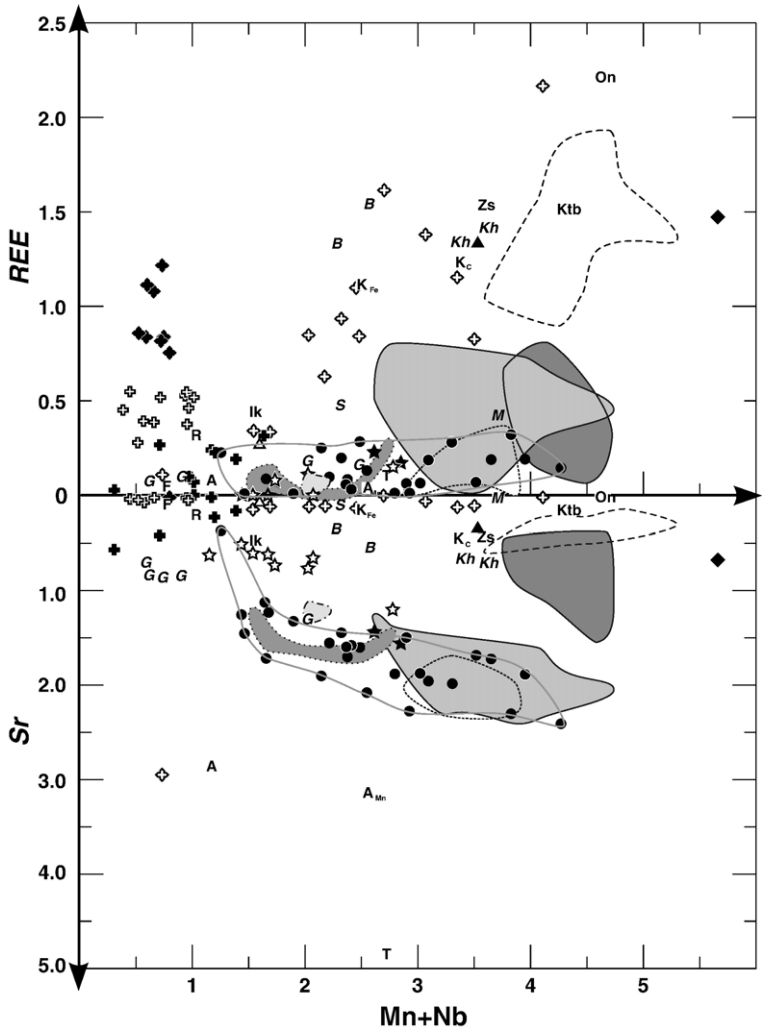

Fig. 5. Compositional variations of eudialyte (*afu*). See Fig. 4 for legend.

sites than holotype kentbrooksite (Fig. 4a), and many approach 1 afu for Nb and Mn at these structural sites.

In summary, eudialyte-II in the heterogeneous lujavrite exhibits an extremely wide range in composition from ferroan manganoan eudialyte, similar to eudialyte-I, through kentbrooksite to taseqite-like varieties enriched in Sr, Nb and REE. Some of the eudialyte-II compositions are similar to those of eudialyte-I and might be relict primary material. Individual grains have discrete compositions, and the wide compositional variation is attributed to cation exchange during interaction of primary eudialyte-I (and -II) with deuteric fluids during the formation of type 2 replacement assemblages. This hypothesis is supported by the development of diffuse but quite different fields of eudialyte-II compositions plotted in the $Nb_{M(3)}$ versus $Mn_{M(2)}$ diagram (Fig. 4a).

Eudialyte-III in lujavrite has the *M*(3) site populated only by Nb and falls entirely in the kentbrooksite quadrant in the $Nb_{M(3)}$ versus $Mn_{M(2)}$ diagram (Fig. 4a). In addition, it contains from 4.3 to 7.3 wt.% SrO (Table 4, comp. 12–13) and is the most REE-poor variety of hydrothermal eudialyte-III in the Pilansberg lujavrites (<1.9 wt.% REE_2O_3). In contrast, eudialyte-III replacing Na–Zr-silicate and zircon in melanolujavrite, is not strontian but extremely rich in REE, Mn and Nb (Figs. 4b and 5), and contains up to 9.1 wt.% REE_2O_3 (Ce>La) and 8.3 wt.% MnO (Table 4, comp. 14–15). The most manganoan samples approach oneillite in terms of cationic proportions (Johnsen et al., 2003a) when Mn assigned to the *M*(1) site reaches <2.5 afu. A plot of (Mn+Nb) versus REE shows a near-linear trend of enrichment in lanthanides from eudialyte-II to eudialyte-III in melanolujavrite, a trend that is not characteristic of eudialyte from other Pilansberg

lujavrites (Figs. 4b and 5). The most Sr–Nb-rich compositions found for the hydrothermal generation of eudialyte-III in terms of $Nb_{M(3)}$ (≫0.5 afu Nb) and $Sr_{N(4)}$ (~2.3 afu Sr) are transitional to taseqite (Petersen et al., 2004).

We consider on the basis of composition and petrographic data that the eudialyte occurring in a Pilansberg melanolujavrite studied by Olivo and Williams-Jones (1999) belongs to our eudialyte-III group. Unfortunately, their data cannot be usefully compared with ours as Sr was not analysed in their study.

The small size of the eudialyte grains does not permit determination of anion composition. Development of carbonates (strontianite, REE-carbonates and fluorocarbonates), fluorite and abundant deuteric (zeolites and other postmagmatic phases) mineralization coeval with eudialyte-II and eudialyte-III suggests the possible presence of unaccounted CO_3^{2-} and OH^- groups in the eudialyte studied, and thus the probable occurrence of carbokentbrooksite and carbonic and/or fluoro-analogs of taseqite and oneillite.

8. Fluids and deuteric alteration

We propose that the textural and mineralogical variations observed in the Pilansberg lujavrites result from rheological controls on crystal sorting, accumulation, lamination and magmatic foliation in low viscosity lujavrite-forming magmas (e.g. Féménias et al., 2005), followed by extensive low temperature postmagmatic alteration of both primary and secondary minerals by hydrous Na–Cl-bearing fluids.

Typically, agpaitic magmas have an extended crystallization interval and the solidus might occur at temperatures as low as 450 °C (Sood and Edgar, 1970; Larsen and Sørensen, 1987; Markl, 2001; Markl and Baumgartner, 2002). At the Ilímaussaq and Lovozero complexes, there occur low temperature (<450 °C) late-magmatic-to-hydrothermal veins consisting of analcime, albite and aegirine together with ussingite and other sodic aluminosilicates. The fluids from which these veins and pegmatites formed are considered to have been sodic, aqueous and basic (Markl and Baumgartner, 2002). Khomyakov (1995) has devised a generalized paragenetic model for the mineral assemblages developed from such evolving fluids on the basis of an empirical parameter termed the alkalinity modulus (K_{alk}). The latter is calculated from the structural formulae of typomorphic minerals present in a particular vein assemblage and is a parameter, which reflects the relative "agpaicity" of the assemblage present. Khomyakov (1995) recognises miaskitic, agpaitic and hyperagpaitic assemblages, which are formed as the mineral-forming fluids evolve towards increasing sodium and water contents. In practice, the typomorphic mineral assemblages defined for each alkalinity modulus by Khomyakov (1995) can be used to assess the degree of "agpaicity" of any particular mineral paragenesis. Markl and Baumgartner (2002) have developed a quantitative model to explain the mineral assemblages observed in autometasomatically altered lujavrite in terms of changes in the Na/Cl ratio, pH and temperature of the fluids.

Our petrographic data show that the primary mineral assemblages of the Pilansberg lujavrites have undergone extensive subsolidus low temperature re-equilibration with deuteric fluids. Unlike most other agpaitic complexes, these fluids have apparently not separated into discrete pegmatites and hydrothermal veins, but have been retained in situ. Deuteric alteration took place in several episodes as the composition and pH of the fluid evolved by reaction with pre-existing minerals and decreasing temperature. Alteration apparently occurred under conditions such that volume was conserved.

Fig. 6 presents the generalized paragenetic sequence deduced for the formation of primary (stage I) and deuteric (stages II–V) mineral assemblages in Pilansberg lujavrite. In terms of the Khomyakov (1995) model, the "agpaicity" of the orthomagmatic agpaitic mineral-forming *milieu* was followed by a miaskitic fluid which than evolved through agpaitic to hyperagpaitic and ultimately back to agpaitic and miaskitic compositions. According to the model of Markl and Baumgartner (2002), such a sequence of assemblages reflects increasing pH from the miaskitic (stage II) to the agpaitic and hyperagpaitic stages (stages III–IV) followed by decreasing pH in the ultimate low agpaitic-to-miaskitic fluids from which a SiO_2 mineral phase was ultimately precipitated (stage V). The changes in pH reflect changes in the Na/Cl of the fluids in response to reaction of these fluids with eudialyte, sodalite, nepheline and feldspars.

Initial postmagmatic alteration (stage II in Fig. 6) of sodalite and eudialyte released Cl, Na and Zr leading to the formation of a miaskitic assemblage characterized by the crystallization of zircon, pyrochlore, britholite, fergusonite-(Ce) and allanite-(Ce) coupled with a decrease in the Na/Cl ratio of the fluids. At termination of the stage II, after the Na/Cl buffer was exhausted due to complete alteration of sodalite and eudialyte-I, alkalinity was increased as documented by the repeated formation of "agpaitic" minerals such as eudialyte-II and lamprophyllite. Stage III mineral assemblages consist principally of analcime, deuteric Na–Zr-silicates and numerous sodic microphases. The absence of Cl-bearing

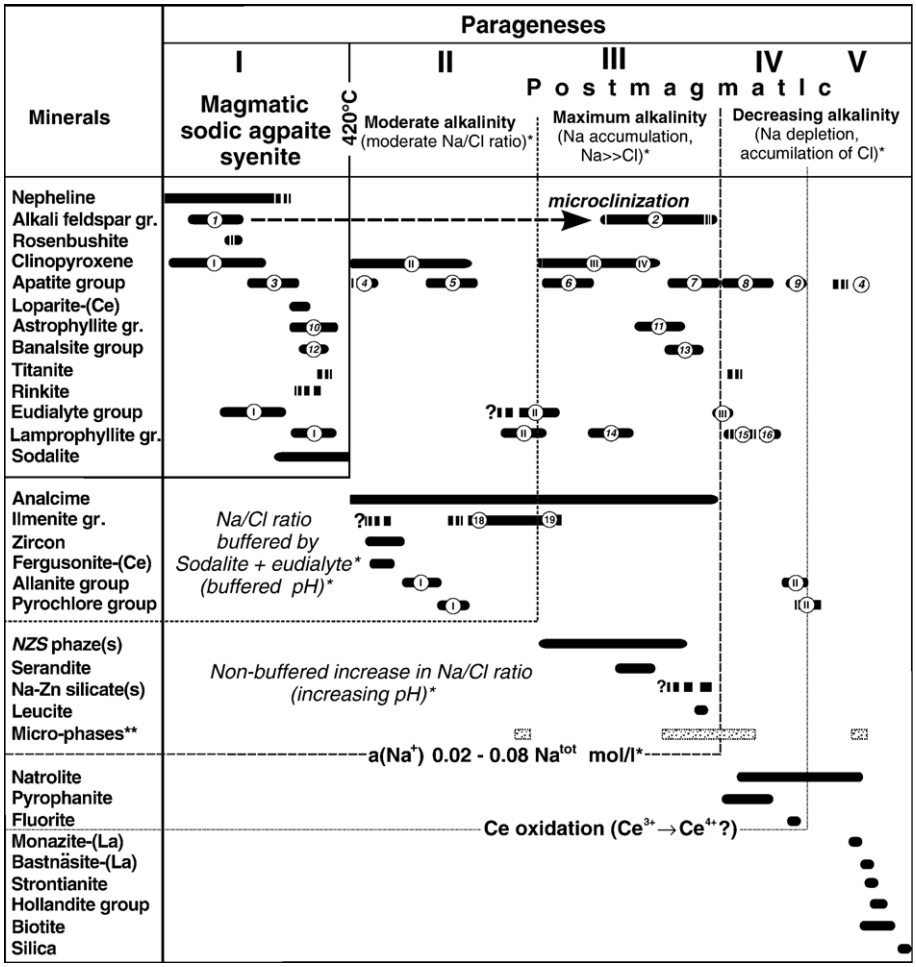

Fig. 6. Generalized sequence of formation and alteration of lujavrite in the Pilansberg complex, South Africa. See Markl and Baumgartner (2002) for details of the pH evolution path of sodic fluids related to lujavrites. NZS = an unidentified deuteric Na–Zr–Si phase(s). Mineral generations are given in Roman numerals. Species recognized within mineral groups are as follows (marked in Arabic numerals, in italics): (1) alkali feldspar(s), unspecified, (2) high microcline, (3) fluorapatite, (4) britholite-(Ce), (5) strontian fluorapatite, (6) a fluoro-analog of strontium-apatite, (7) REE-bearing strontium-apatite, (8) belovite-(Ce), (9) REE-bearing fluorapatite, (10) astrophyllite, (11) kupletskite, (12) banalsite, (13) stronalsite, (14) lamprophyllite, (15) barytolamprophyllite, (16) hejtmanite, (17) delindeite, (18) ecandrewsite, (19) zincian pyrophanite, (20) pyrophanite.

minerals suggests that the Na/Cl ratio of the fluid was not buffered and increased, resulting in an increase in pH and a change from agpaitic to hyperagpaitic mineral assemblages. The increase in Na is considered to result principally from the alteration of nepheline. At this stage, eudialyte-II also underwent cation exchange and alteration. Stage IV marks a decrease in the Na/Cl ratio as substantial amounts of natrolite, Na–Zr-silicate and other sodic phases were precipitated and/or replaced nepheline, analcime and alkali feldspar. During this stage and the transition to stage V, hydrothermal eudialyte-III and clinopyroxene-IV (aegirine) mantled pre-existing eudialyte-II (Fig. 3f), and replaced Na–Zr-silicates (Fig. 3g, h). Pyrophanite, fluorite, britholite, pyrochlore and allanite-(La) were also deposited during stage IV. Subsequently, the mineral assemblage changed from low agpaitic to miaskitic in stage V with the continued deposition of natrolite. The final, presumably very low temperature, fluids became relatively acidic as Na/Cl continued to fall. Coupled with this decrease in pH, there was oxidation of Ce^{3+} to Ce^{4+}, and fractionation of the REE such that allanite-(La), monazite-(La) and bastnäsite-(La) were precipitated. The final phases to crystallize were a SiO_2 mineral phase (polymorph unknown) and manganoan biotite, the latter replacing aegirine, amphibole and ilmenite group minerals.

Our interpretation of the evolution of the deuteric fluids associated with the Pilansberg lujavrites suggests that pH first decreased, increased to a hyperalkaline level and then decreased again. This conclusion differs

from the simple increase in the pH of the hydrothermal veins associated with the Ilímaussaq complex postulated by Markl and Baumgartner (2002). The difference is considered to be due to the retention of the residual fluids in the Pilansberg lujavrites and increased opportunities for mineral–fluid interaction.

Complex subsolidus alteration of eudialyte seems to be characteristic of agpaitic complexes. Apart form this work, there have been few detailed investigations of this process. Coulson (1997) has shown that eudialyte at North Qôroq is replaced by zircon, allanite-(Ce), aegirine, natrolite, titanite, rinkite, møsandrite, wöhlerite and zirfesite. This assemblage can be described as miaskitic and corresponds to stage II alteration at Pilansberg. At Gordon Butte (Montana), eudialyte is partially replaced by calcium catapleiite and REE-carbonates, and Chakhmouradian and Mitchell (2002) note the pH of the late-stage fluid remained relatively low and that the pegmatite-forming fluid never reached the hyperagpaitic stage. It is not known why alteration terminated at the miaskitic stage or why low temperature basic fluids were not produced at North Qôroq and Gordon Butte, although this might be related to either the absence of sodalite or the relatively limited alteration of nepheline in these syenites.

9. Conclusions

Pilansberg lujavrites have undergone extensive subsolidus low temperature (<450 °C) equilibration with deuteric Na and Cl-rich hydrothermal fluids. The primary minerals, alkali feldspar, nepheline, sodalite and eudialyte, have been replaced by complex assemblages of secondary minerals. Three types of alteration and replacement of eudialyte have been recognized and the mineral assemblages formed are considered to reflect the Na/Cl ratio and pH of the deuteric fluids whose composition changes continuously as a result of reactions with both primary and secondary minerals. The latter, in sequence, range from an initial miaskitic assemblage, through agpaitic and hyperagpaitic types, with a return to low agpaitic and miaskitic assemblages in the final stages of alteration.

Acknowledgements

This work was supported by the Natural Sciences and Engineering Research Council of Canada and Lakehead University. Allan MacKenzie and Anne Hammond are thanked for assistance with the analytical work and sample preparation, respectively. Dr. R.C. (Jock) Harmer is thanked for assistance with the collection of the Pilansberg syenites. The Director of the Pilansberg National Park is thanked for permission to undertake geological investigations in the park area. Constructive reviews by Ian Coulson and Henning Sørensen contributed to improvement of the manuscript. The editorial care of Gregor Markl is highly appreciated.

Appendix A. Theoretical formulae of some of the less-common minerals mentioned in the text

Mineral	An idealized formula	
Allanite-(Ce)	$(Ca,Ce)_2(Al,Fe^{2+},Fe^{3+})_3(SiO_4)(Si_2O_7)O(OH)$	
Allanite-(La)	$(Ca,La,Ce,)_2(Fe^{2+},Mn^{2+},\ Al,Fe^{3+})_3(SiO_4)(Si_2O_7)O(OH)$	
Ancylite-(Ce)	$SrCe(CO_3)_2(OH)\cdot(H_2O)$	
Ancylite-(La)	$Sr(La,Ce)(CO_3)_2(OH)\cdot(H_2O)$	
Astrophyllite	$K_2Na(Fe^{2+},Mn)_7Ti_2Si_8O_{26}(OH)_4F$	
Banalsite	$BaNa_2Al_4Si_4O_{16}$	
Barytolamprophyllite	$(Na,K)_3(Ba,Fe^{2+},Ca)_2(Ti,Fe^{3+})_3O_2(Si_2O_7)_2(F,OH,O)_2$	
Belovite-(Ce)	$NaRESr_3(PO_4)_3(F,OH)$	
Betafite	$(Na,Ca,REE,Sr,U,Th)_{2-x}(Nb,Ti,Si_{(?)})O_6(F,OH)_{1-y}$ Nb/Ti<2	$x\sim0–2$, $y\sim0–1$
Britholite-(Ce)	$(Ce,La,Sr,Ca)_5(SiO_4,PO_4)_3(OH,F)$	
Burbankite	$(Na,Ca)_3(Sr,Ba,Ce)_3(CO_3)_5$	
Carbokentbrooksite	$(Na,[])_{12}(Na,Ce)_3Ca_6Mn_3Zr_3Nb(Si_{25}O_{73})(OH)_3(CO_3)\cdot H_2O$	
Coronadite	$Pb(Mn,Mn)_8O_{16}$	
Delindeite	$(Na,K)_3(Ba,Ca)_4(Ti,Fe,Al)_6Si_8O_{26}(OH)_{14}$	
Deloneite-(Ce)	$NaCa_2Sr(Ce,La,Pr)(PO_4)_3F$	
Ecandrewsite	$(Zn,Mn,Fe)TiO_3$	
Ferrokentbrooksite	$Na_{15}Ca_6(Fe,Mn)_3Zr_3NbSi_{25}O_{73}(O,OH,H_2O)_3(Cl,F,OH)_2$	
Feklichevite	$Na_{11}Ca_9(Fe^{3+},Fe^{2+})_2Zr_3Nb[Si_{25}O_{73}](OH,H_2O,Cl,O)_5$	
Fergusonite-(Ce)	$(Ce,Nd,La)NbO_4\cdot nH_2O$	$n\sim0.3$
Fluorcaphite	$Ca(Sr,Na,Ca)(Ca,Sr,Ce)_3(PO_4)_3F$	

Appendix A (*continued*)

Gasparite-(Ce)	$(Ce,La,Nd)AsO_4$	
Hejtmanite	$Ba(Mn^{2+},Fe^{2+})_2TiO(Si_2O_7)(OH,F)_2$	
Ikranite	$(Na,H_3O)_{15}(Ca,Mn,REE)_6Fe^{3+}{}_2Zr_3([],Zr)([],Si)Si_{24}O_{66}(O,OH)_6Cl{\cdot}nH_2O$	$n\sim2$–3
Keldyshite	$Na_3HZr_2(Si_2O_7)_2$	
Kentbrooksite	$(Na,REE)_{15}(Ca,REE)_6Mn_3Zr_3NbSi_{25}O_{74}F_2{\cdot}2H_2O$	
Khomyakovite	$Na_{12}Sr_3Ca_6Fe_3Zr_3W(Si_{25}O_{73})(O,OH,H_2O)_3(OH)_2$	
Kupletskite	$K_2Na(Mn,Fe^{2+})_7Ti_2Si_8O_{26}(OH)_4F$	
Lamprophyllite	$(Na,Mn,K)_3(Sr,Ba)_2Ti_3O_2(Si_2O_7)_2(O,OH,F)_2$	
Loparite-(Ce)	$(Na,REE,Ca,Sr,Th)(Ti,Nb,Fe^{2+})O_3$	
Manganokhomyakovite	$Na_{12}Sr_3Ca_6Mn_3Zr_3W(Si_{25}O_{73})(O,OH,H_2O)_3(OH)_2$	
Natrolite	$Na_2Al_2Si_3O_{10}{\cdot}2H_2O$	
Naujakasite	$Na_6(Fe^{2+},Mn^{2+})Al_4Si_8O_{26}$	
Olekminskite	$Sr(Sr,Ca,Ba)(CO3)_2$	
Oneillite	$Na_{15}Ca_3Mn_3Fe_3Zr_3Nb(Si_{25}O_{73})(O,OH,H_2O)_3(OH,Cl)_2$	
Parakeldyshite	$Na_2ZrSi_2O_7$	
Paraumbite	$K_3Zr_2HSi_6O_{18}{\cdot}nH_2O$	$n\sim7$–8
Pyrochlore	$(Na,Ca,REE,Sr,U,Th)_{2-x}(Nb,Ti,Si_{(?)})O_6(F,OH)_{1-y}$ Nb/Ti>2	$x\sim0$–2, $y\sim0$–1
Raslakite	$Na_{15}Ca_3Fe_3(Na,Zr)_3Zr_3(Si,Nb)(Si_{25}O_{73})(OH,H_2O)_3(Cl,OH)$	
Rengeite	$Sr_4ZrTi_4Si_4O_{22}$	
Retzian-(Ce)	$Mn_2CeAsO_4(OH)_4$	
Rinkite	$(Ca,Ce)_4Na(Na,Ca)_2Ti(Si_2O_7)_2F_2(O,F)_2$	
Rosenbushite	$(Ca,Na)_3(Zr,Ti)Si_2O_7(O,F)_2$	
Sérandite	$Na(Mn^{2+},Ca)_2Si_3O_8(OH)$	
Sodalite	$Na_8Al_6Si_6O_{24}Cl_2$	
Stronalsite	$Na_2SrAl_4Si_4O_{16}$	
Strontium-apatite	$(Sr,Ca)_5(PO_4)_3(OH,F)$	
Tainiolite	$KLiMg_2Si_4O_{10}F_2$	
Taseqite	$Na_{12}Sr_3Ca_6Fe_3Zr_3NbSi_{25}O_{73}(O,OH,H_2O)_3Cl_2$	
Ussingite	$Na_2AlSi_3O_8(OH)$	
Wöhlerite	$NaCa_2(Zr,Nb)Si_2O_7(O,OH,F)_2$	
Zirsilite-(Ce)	$(Na,[])_{12}(Ce,Na)_3Ca_6Mn_3Zr_3Nb(Si_{25}O_{73})(OH)_3(CO_3){\cdot}H_2O$	

References

Bussen, I.V., Sakharov, A.C., 1972. The Petrology of the Lovozero Alkaline Massif. Nauka Press, Leningrad (in Russia). 296 pp.

Chakhmouradian, A.R., Mitchell, R.H., 2002. The mineralogy of Ba- and Zr-rich pegmatites from Gordon Butte, Crazy Mountains (Montana, USA): comparison between potassic and sodic agpaitic pegmatites. Contrib. Mineral. Petrol. 143, 93–114.

Coulson, I.M., 1997. Postmagmatic alteration in eudialyte from the North Qôroq centre, South Greenland. Mineral. Mag. 61, 99–109.

Chukanov, N.V., Pekov, I.V., Zadov, A.E., Korovushkin, V.V., Ekimenkova, I.A., Rastsvetaeva, R.K., Khasanov, V.V., 2003. Ikranite, $(Na,H_3O)_{15}(Ca,Mn,REE)_6Fe^{3+}_2Zr_3([],Zr)([],Si)$ $Si_{24}O_{66}(O,OH)_6Cl{\cdot}nH_2O$, and raslakite, $Na_{15}Ca_3Fe_3(Na,Zr)_3Zr_3(Si,Nb)(Si_{25}O_{73})(OH,H_2O)_3(Cl,OH)$—new eudialyte-group minerals from the Lovozero massif, Kola Peninsula (in Russian) Zap. Vseross. Mineral. Obshchest 132 (5), 22–33.

Dollase, W.A., Thomas, W.M., 1978. The crystal chemistry of silica-rich, alkali-deficient nepheline. J. Petrol. 20, 311–318.

Droop, G.T.R., 1987. A general equation for estimation of Fe^{3+} concentrations in ferromagnesian silicates and oxides from microprobe analyses using stoichiometric criteria. Mineral. Mag. 51, 431–435.

Féménias, O., Coussaert, N., Brassinnes, S., Demaiffe, D., 2005. Emplacement processes and cooling history of layered cyclic unit II-7 from the Lovozero alkaline massif (Kola Peninsula, Russia). Lithos 83, 371–393.

Ferguson, J., 1973. The Pilansberg alkaline province. Trans. Geol. Soc. S. Afr. 76, 207–214.

Hamilton, D.L., 1961. Nephelines as crystallization temperature indicators. J. Geol. 69, 321–329.

Johnsen, O., Grice, J.D., 1999. The crystal chemistry of the eudialyte group. Can. Mineral. 37, 865–891.

Johnsen, O., Grice, J.D., Gault, R.A., 1998. Kentbrooksite from the Kangerdlugssuaq intrusion, East Greenland, a new Mn–REE–Nb–F end-member in a series within eudialyte group: description and crystal structure. Eur. J. Mineral. 10, 207–219.

Johnsen, O., Ferraris, G., Gault, R.A., Grice, J.D., Kampf, A.R., Pekov, I.V., 2003a. The nomenclature of eudialyte-group minerals. Can. Mineral. 41, 785–794.

Johnsen, O., Gault, R.A., Grice, J.D., 2003b. Ferrokentbrooksite, a new member of the eudialyte group from Mont Saint-Hilaire, Quebec. Can. Mineral. 41, 55–60.

Khomyakov, A.P., 1995. Mineralogy of Hyperagpaitic Alkaline Rocks. Oxford science publications, Clarendon Press. 223 pp.

Khomyakov, A.P., Sørensen, H., Petersen, O.V., Bailey, J.C., 2001. Naujakasite from the Ilímaussaq alkaline complex, South Greenland and the Lovozero alkaline complex, Kola Peninsula, Russia: a comparison. In: Sørensen, H. (Ed.), The Ilímaussaq Complex, South Greenland: Status of Mineralogical Research with New Results. Geol. Greenl. Surv. Bull., vol. 190, pp. 95–108.

Kohmyakov, A.P., Dusmatov, V.D., Ferraris, G., Gula, A., Ivaldi, G., Nechelyustov, G.N., 2003. Zirsilite-(Ce), $(Na,[])_{12}(Ce,Na)_3Ca_6$

$Mn_3Zr_3Nb(Si_{25}O_{73})(OH)_3(CO_3)\cdot H_2O$, and carbo-kentbrooksite, $(Na,[])_{12}(Na,Ce)_3Ca_6Mn_3Zr_3Nb(Si_{25}O_{73})(OH)_3(CO_3)\cdot H_2O$—two new eudialyte-group minerals from the Dara-i-Pioz alkaline massif, Tajikistan (in Russian) Zap. Vseross. Mineral. Obshchest 132 (5), 40–51.

Kostyleva-Labuntsova, E.E., Borutsky, B.E., Sokolova, M.N., Shlyukova, Z.V., Dorfman, M.D., Dudkin, O.B., Kozyreva, L.V., 1978. Mineralogy of Khibina Complex, Part II. Nauka, Moscow (in Russian). 585pp.

Larsen, L.M., Sørensen, H., 1987. The Ilímaussaq intrusion—progressive crystallization and formation of layering in an agpaitic magma. In: Fitton, J.G., Upton, B.G.J. (Eds.), Alkaline Igneous Rocks. Geol. Soc. Spec. Publ., vol. 30, pp. 473–488.

Lurie, J., 1973. The Pilanesberg: geology, rare element geochemistry and economic potential. PhD thesis (unpubl.). Rhodes. Univ., Grahamstown. 308 pp.

Lurie, J., 1986. Mineralization of the Pilansberg alkaline complex. In: Anhaeusser, C.R., Maske, S. (Eds.), Mineral Deposits of South Africa, vol. 2. The Geological Society of South Africa, Johannesburg, South Africa, pp. 2215–2228.

Markl, G., 2001. A new type of silicate liquid immiscibility in peralkaline nepheline syenites (lujavrites) of the Ilímaussaq complex, South Greenland. Contrib. Mineral. Petrol. 141, 458–472.

Markl, G., Baumgartner, L., 2002. pH changes in peralkaline late-magmatic fluids. Contrib. Mineral. Petrol. 144, 331–346.

Marks, M., Markl, G., 2003. Ilímaussaq 'en miniature': closed-system fractionation an agpaitic dyke rock from the Gardar Province, South Greenland (contribution to the mineralogy of Ilímaussaq no. 117). Mineral. Mag. 67, 893–919.

Mitchell, R.H., 1996. Classification of undersaturated and related alkaline rocks. In: Mitchell, R.H. (Ed.), Undersaturated Alkaline Rocks: Mineralogy, Petrogenesis and Economic Potential. Mineral. Assoc. Can., vol. 24, pp. 1–22.

Mitchell, R.H., Liferovich, R.P., 2004. Ecandrewsite-zincian pyrophanite from lujavrite, Pilansberg alkaline complex, South Africa. Can. Mineral. 42, 1169–1178.

Mitchell, R.H., Platt, R.G., 1979. Nepheline-bearing rocks from the Poohbah Lake complex, Ontario: malignites and malignites. Contrib. Mineral. Petrol. 69, 255–264.

Mitchell, R.H., Platt, R.G., 1982. Mineralogy and petrology of nepheline syenites from the Coldwell alkaline complex, Ontario, Canada. J. Petrol. 23, 186–214.

Mitchell, R.H., Vladykin, N.V., 1996. Rare-earth element-bearing tausonite and barium titanates from the Little Murun potassic alkaline complex, Yakutia, Russia. Mineral. Mag. 57, 651–664.

Olivo, G.R., Williams-Jones, A.E., 1999. Hydrothermal REE-rich eudialyte from the Pilansberg complex, South Africa. Can. Mineral. 37, 653–663.

Pekov, I.V., Ekimenkova, I.A., Chukanov, N.V., Rastsvetaeva, R.K., Kononkova, N.N., Pekova, N.A., Zadov, A.E., 2001. Feklichevite, $Na_{11}Ca_9(Fe^{3+},Fe^{2+})_2Zr_3Nb[Si_{25}O_{73}](OH,H_2O,Cl,O)_5$, a new mineral of the eudialyte group from the Kovdor massif, Kola Peninsula (in Russian) Zap. Vseross. Mineral. Obšestva 130 (3), 55–65.

Petersen, O.V., Johnsen, O., Gault, R.A., Niedermayr, G., Grice, J.D., 2004. Taseqite, a new member of the eudialyte group from the Ilímaussaq alkaline complex, South Greenland. Neues Jahrb. Mineral., Monatsh. 2, 83–96.

Piilonen, P.C., Lalonde, A.E., McDonald, A.M., Gault, R.A., Larsen, A.O., 2003. Insights into astrophyllite-group minerals: I. Nomenclature, composition and development of a standardized general formula. Can. Mineral. 41, 1–26.

Ramsay, W., 1894. Die Nephelinsyenitmassiv. In: Ramsay, W., Hackman, V. (Eds.), Das Nephelinsyenitgebiet auf der Halbsinsel Kola. Fennia, vol. 9, pp. 89–94.

Retief, E.A., 1962. Preliminary observations on the feldspars from the Pilanesberg alkaline complex, Transvaal, S. Africa. Nor. Geol. Tidsskr. 42 (2), 493–513.

Retief, E.A., 1963. Petrological and mineralogical studies in the southern part of the Pilansberg complex, Transvaal, South Africa. PhD thesis, Univ. of Oxford, Oxford, U.K.

Rose-Hansen, J., Sørensen, H., 2002. Geology of the Lujavrites from the Ilímaussaq alkaline complex, South Greenland, with information from seven bore holes. (contribution to the mineralogy of Ilímaussaq no. 109) Meddel. Grønland Geosci. 40, 58 pp. downloaded at http://www.dpc.dk/PolarPubs/MoG/Dokumenter/Geo40.pdf.

Shand, S.I., 1928. The geology of Pilansberg in the western Transvaal. Trans. Geol. Soc. S. Afr. 31, 91–156.

Sood, M.K., Edgar, A.D., 1970. Melting relations of undersaturated alkaline rocks. Medd. Grønl. 181.

Wilkinson, J.F.G., 1965. Some feldspars, nephelines and analcimes from the Square Top intrusion. Contrib. Mineral. Petrol. 106, 124–128.

Wilkinson, J.F.G., Hensel, H.D., 1994. Nephelines and analcimes in some alkaline igneous rocks. Contrib. Mineral. Petrol. 118, 79–91.

Woolley, A.R., Platt, R.G., 1986. The mineralogy of nepheline syenite complexes from the northern part of the Chilwa Province, Malawi. Mineral. Mag. 50, 597–610.